Research Square

Preprints are preliminary reports that have not undergone peer review.
They should not be considered conclusive, used to inform clinical practice,
or referenced by the media as validated information.

Systems genetics implicate the key mitochondrial gene Nrf1 in the build-up of sleep pressure in mice

Carlos Neves

carloseduardo.sousaneves@unil.ch

University of Lausanne https://orcid.org/0000-0002-3314-2166

Sonia Jimenez

University of Lausanne

Yann Emmenegger

Center for Integrative Genomics, University of Lausanne

Charlotte Hor

University of Lausanne

Paul Franken

University of Lausanne https://orcid.org/0000-0002-2500-2921

Article

Keywords: Sleep homeostasis, EEG delta power, ATAC-seq, QTL, Drp1/Dnm1l, Nrf1, mitochondria, Mus musculus

Posted Date: June 3rd, 2026

DOI: https://doi.org/10.21203/rs.3.rs-9589050/v1

License: This work is licensed under a Creative Commons Attribution 4.0 International License.
Read Full License

Additional Declarations: There is **NO** Competing Interest.

Systems genetics implicate the key mitochondrial gene *Nrf1* in the build-up of sleep pressure in mice

Abstract

Individual differences in resilience to the impact of sleep deprivation (SD) imply genetic and molecular factors contributing to the cognitive and physiological dysregulation associated with increased sleep pressure. SD's impact has, however, been studied mostly at one molecular levels and in one genetic background. Using the BXD mouse genetic reference population, we show that SD results in wide-spread alterations in chromatin accessibility in the cerebral cortex. We integrated these findings with genomic, transcriptomic, and phenotypic data to infer the genetic and gene-regulatory network of the SD response; SD-Net. SD-Net revealed a centralized early transcriptional response to SD with genetic variation influencing downstream factors, providing a conceptual model explaining the observed independent inheritance of distinct sleep phenotypes. SD-Net further identified *Nrf1* as central regulator of sleep pressure. We could validate *Nrf1*'s role, but not that of *Dnm1l*, implicating mitochondrial biogenesis rather than fission in the intracellular processes governing sleep homeostasis.

Keywords: *Sleep homeostasis, EEG delta power, ATAC-seq, QTL, Drp1/Dnm1l, Nrf1, mitochondria, Mus musculus*

Abbreviations

ATAC: Assay for Transposase-Accessible Chromatin

B6: C57BL/6J mouse inbred strain

BXD: GRP of advanced recombinant inbred lines derived from B6 and D2

cCRE: Candidate Cis Regulatory Elements

D2: DBA/2J mouse inbred strain

DAR: Differentially accessible Regions

ELS: ENCODE Enhancer-Like Element

ENCODE: Encyclopedia of DNA Elements

GR-sNet: Gene Regulatory sub-network

GRP: Genetic Reference Population

GSEA: Gene Set Enrichment Analysis

h: hour

icKO: Inducible and conditional KO

IEG: Immediate Early Gene

KEA: Kinase Enrichment Analysis

KO: Knock-out mutant

LOD: Log of Odds Ratio

QTL: Quantiltative trait locus

aQTL*:* accessibility QTL

aQTLxSD: QTL for accessibility fold-change (interaction)

eQTL: expression QTL

eQTLxSD: QTL for expression fold-change (interaction)

pQTL: phenotype QTL

SD: sleep deprivation

SD-Net: Inferred genetic and gene-regulatory network for the response to SD

SG-sNet: System Genetics sub-network

SNP: Single Nucleotide Polymorphism

TF: Transcription Factor

TSS: Transcriptional Start Site

ZT: Zeitgeber Time

Introduction

The fundamental evolutionary functions of sleep still remain a matter of debate, with a multitude of distinct hypotheses having been proposed [1–4]. Despite this variety, these hypotheses all share the core idea that wakefulness drives the system away from an optimal and sustainable physiological state, thereby incurring an imbalance only sleep can homeostatically correct [5]. These deficits in sleep impair cognitive performance, including memory and learning [6,7], and reduce alertness, which in turn increases the likelihood of accidents [8] and reduced survival fitness. Moreover, chronic sleep deficit is associated with increased risk of disease such as metabolic syndrome and neurodegeneration [9–14]. These physiological and pathological effects are thought to be related to the sleep-wake-driven molecular changes found throughout the organism, a view which is supported by the observation that many aspects of sleep, including its homeostatic regulation, are under strong genetic control [15,16], implying at least a partial molecular origin. In agreement, gene targeting studies and mutagenesis screens have demonstrated that single genes can have large effects on various aspects of sleep [17–19]. However, such large, single-gene effects are rare in the human population, likely due to the physiological importance of sleep and, therefore, strong negative selective pressure. Instead, phenotypic variability is thought to be a product of the interaction of many allelic variants, their epistatic interactions, and their interaction with the environment. To study these complex, non-Mendelian traits, mouse genetic reference populations (GRPs) have been generated, where each line represents a reproducible clone of animals, so that different molecular datasets can be collected and compared at the population level. The currently best characterized murine GRP is the BXD panel of recombinant inbred lines derived from the parental strains C57BL/6J (B6) and DBA/2J (D2) [20], which we have extensively used to chart the transcriptomic, metabolomic, and phenotypic consequences of sleep deprivation (SD) [15,16].

At the molecular level, SD has been shown to induce major changes in the transcriptome [16,21–24], the (phospho-) proteome [25–27], and ion [28–30] and metabolite concentrations [16] in various tissues and species, particularly in the central nervous system. Among the numerous molecular changes, it remains unclear, which are causally implicated in the homeostatic feedback regulation of sleep, and which are merely driven by sleep and waking states. As such, insight into the molecular consequences of SD and the underlying homeostatic regulatory mechanisms is instrumental in advancing our understanding of sleep function and regulation. Focusing on the cerebral cortex, which is both a direct target of sleep loss at the molecular, electrophysiological, and cognitive levels and a proposed substrate of the sleep homeostat [31,32], we extend our system genetics database [16] by quantifying chromatin accessibility using Assay for Transposase-Accessible Chromatin with high-throughput sequencing (ATAC-seq) in the BXD panel under baseline and SD conditions. Changes in chromatin accessibility provide an aggregated view into the epigenetic changes, representing a central mechanism of gene regulation [33] and a key point for multiomic integration analysis of the response to SD, the description of which is currently lacking. We show that enforced periods of wakefulness alter chromatin accessibility congruently with gene expression, generalizing our previous results in B6 mice to other genetic backgrounds [34]. We further find that not just transcription levels, but also chromatin state and the effects of SD thereon, are widely influenced by genetic variability. To gain insight into the integrated molecular response to SD and the influence of genetic variability on various aspects of sleep, we derived a genetic and gene-regulatory network for the response to SD (SD-Net) using the available data from the BXD population. This framework allowed us to explore cortical molecular responses to

SD and identify factors associated with multiple phenotypical aspects of sleep-wake regulation. Of these, we experimentally validated the nuclear respiratory factor 1 (*Nrf1*), confirming it as an important contributor to the regulation of sleep pressure build-up during SD, thereby placing mitochondrial biogenesis at the core of sleep homeostasis. However, when comparing the effects to those of dynamin-1-like protein (*Dnm1l/Drp1*) mutants, a gene required for mitochondrial fission and recently implicated in sleep regulation in *Drosophila* [35,36], we find that in the mouse, the mitochondrial effects on sleep are multifaceted, with *Dnm1l* influencing only a subset of the *Nrf1* phenotypes, but not the sleep homeostatic response.

Results

Sleep deprivation induces extensive changes in chromatin accessibility

Changes in chromatin accessibility are a well-established epigenetic mechanism contributing to the regulation of gene expression. Given the high temporal correlation in the dynamics of cortical chromatin accessibility and transcript levels in undisturbed, sleep deprived (SD), and post-SD recovery conditions previously described in B6 mice [34] we hypothesize that the sleep-wake-dependent gene regulation is mediated in large part by reversible epigenetic mechanisms leading to changes in chromatin accessibility. As such, we extended our previous system genetics database [16] by including the effects of 6h of SD, starting at light onset (*zeitgeber* time 0 - ZT0) on the cerebral cortex's chromatin accessibility in 32 BXD lines (**Figure S1a**) and the two parental lines, B6 and D2.

Contrasting the results of SD mice to that of time-of-day matched (ZT6) controls allowed to sleep *ad libitum* prior to tissue sampling, we identified 35'866 (25'997 non-contiguous) statistically significant Differentially Accessible Regions (DARs). Of these, 25'567 (71%) were more accessible after SD, while 10'299 (29%) were less accessible (**Figure 1a**, **Table S2**). The identified regions are located across the entire genome with no noticeable genomic clustering (**Figure S1b**). Annotation to the nearest Transcription Start Sites (TSSs) indicates that regions which became more accessible after SD are mostly found in intronic (12'441 – 49%), followed by intergenic (7'584 - 30%) and promoter (4'017 - 16%) regions (**Figure 1b**). Exonic (coding) regions represent only 4% (1'039) of all regions identified. On the other hand, of the regions which became less accessible after SD, 35% (3'646) are located within a promoter, with 31% (3'225) within introns, 27% (2'773) are intergenic, and 4% (380) are exonic. Comparing the identified regions to the ENCODE list of candidate cis-Regulatory Elements (cCREs) [37], 40% of the more accessible regions and 58% of the less accessible regions overlap with annotated cCREs. Most of the cCREs identified (**Figure 1b**) corresponded to distal Enhancer-Like Signatures (dELSs; more accessible: 9'736 – 86%; less accessibly: 5'612 – 81%). In addition, CTCF-bound signatures, a well-established insulator shaping chromatin architecture and facilitating chromatin looping [38], were found in significantly higher proportion (χ^2 p-value < 0.0001) for less accessible regions (2'758 – 40%) than for more accessible regions (1'581 – 14%). These results suggest SD extensively affects chromatin accessibility, mostly making DNA more accessible in non-coding, regulatory regions. Decreases in accessibility associate with CTCF signatures, pointing to higher dimensional chromatin conformation changes as potentially important mechanism underlying the response to SD.

If these accessibility changes are functionally relevant, it would be expected that they correlate with the transcript levels of associated genes. Of the 10'011 unique genes to which the 35'866 DARs were annotated, 7'230 (72%) passed the low expression threshold in our previous RNA-seq experiment [16] (*i.e.* are detectable in the cortex) and 5'671 (57%) were also identified as significantly affected by SD at the transcriptional level, corresponding to 35% of all detectable genes in the cortex (**Table S2**). This observation suggests a relationship between the chromatin accessibility and transcriptional changes during SD. In agreement, the correlation between each DAR and the expression of the gene matching the closest TSS, follows a skewed distribution for Pearson ρ coefficients, with a mode of ρ=0.3 (**Figure S1c**). Of these correlations, we identify 4'041 significant correlations (corresponding to 1'691 unique genes) after multiple test correction. We then considered individual cases and find that the correlations between accessibility and transcript levels can result from different types of associations (**Figure S2**): not only from the effect of SD as expected (*e.g. Nrf1*, *Sgsm1*), but also from strong genetic effects (*e.g. Dynlt1c*, *Hjurp*) or a mixture of both (*e.g. Hps1*). In addition, even if SD significantly affected both accessibility and transcription, this did not always result in a significant correlation as is the case for the chr15:37'607'642-37'607'892 region, the most significant DAR detected (**Figure 1a)**. This region annotates to *Ncald,* which encodes a neuronal calcium sensor protein associated with nighttime sleep in flies [39] yet, the change in accessibility does not correlate with *Ncald*'s transcript levels. Highly significant DARs for which accessibility increases with SD and correlate with the levels of their annotated transcript include *Cadm1* (cell adhesion at synapses), *Tshz1* (neuronal identity and negative reinforcement), *Rbfox3*/*NeuN* (neuronal identity, splicing and synaptic plasticity), and *Nrf1* (mitochondrial biogenesis and oxidative phosphorylation). The most significant DARs with decreased accessibility that correlated with the expression of their nearby genes are *Rasl11b* (circadian small GTPase protein), *Dcaf7* (chaperone/scaffold), *Klf4* (neuronal development and chromatin accessibility, and *Ano2* (chloride channel).

Having confirmed that the identified DARs overlap with functional epigenetic signatures and are correlated with transcript levels, we used Gene Set Enrichment Analysis (GSEA [40]) to identify possible molecular functions these DARs might be involved in. Of the 20'530 unique genes to which all 564'071 tested regions annotated to, we considered the 13'860 (68%) which passed the low expression in our previous RNA-seq experiment [16] (*i.e.* cortical expression), and averaged the accessibility fold-change for all regions associated to the same gene (**Table S3**). Given that not all regions are expected to be functionally associated with their annotated transcript, we obtained the most relevant functions by filtering for terms separately enriched for both DARs and transcriptional differences in response to SD (**Figure 1c**). Overall, 28 overlapping terms were identified, 9 of which were related to synapse organization and activity, hormonal response, and memory. Within these terms, we identify the immediately early genes *Arc, Egr2, Fos, Homer1, Npas4, Nr4a1, Nr4a3, Rcan1 and Rheb* [41–45], affected both at the level of accessibility and transcription (**Figure S1d**), suggesting chromatin accessibility changes play a role in the early steps of the SD response.

Chromatin accessibility changes after SD correlate with MAPK signaling and AP-1 activity

Chromatin accessibility regulates transcription levels by allowing or preventing the activity of DNA-binding factors, such as transcription factors (TFs), co-factors, and the transcriptional machinery. However, the binding of these proteins to accessible chromatin protects it, reducing the number of reads in the ATAC signal, which leaves a detectable transcriptional footprint [46]. We analyzed these footprints to estimate the overall activity of each TF by matching detectable footprints within all

DARs to known TF-binding motifs (**Table S4**). Despite variability among the BXD lines, the estimated TF activities show a clear separation of SD and control samples (**Figure 2a**). In addition, our results also highlight genetic differences, clustering the BXD lines studied into three separated baseline transcriptional states, as well as a cluster of samples (BXD51, BXD44, BXD73) expected to have lower activity for TFs such as FOS and JUN after SD. Aggregation of these results (**Figure 2b**) identify changes in the activity of 92 transcription complexes (79 unique proteins), of which 34 are predicted to increase, and 58 to decrease activity after SD. Of those showing increased activity, 21 (62%) are AP1-related factors (FOS, JUN, BATF). These factors are involved in immediate signaling following neural activity, which is higher during wake than sleep, and their activity can therefore be expected to increase with SD. Given that some of the identified TFs show specificity according to genetic background, we considered which factors were consistently responding to SD. Of the 34 BXD lines studied, there were 13 TFs reaching significance in at least 30 lines (ARNTL, BHLHE40, BHLHE41, CTCFL, HES2, HINFP, JUND, ZBTB33), 5 of which were affected in every line (HES1, KLF15, NRF1, TCFL5, ZBTB14). Of these genes, BHLHE41 (DEC2) is considered a circadian gene which has established causal relationship with human familial natural short sleep [47] and ARNTL (BMAL1) is a central circadian gene [48], that is also affected by SD [34,49]. However, none of the 5 TFs affected by SD in all 34 BXD lines has, to our knowledge, been associated directly with sleep regulation, but have been implicated in memory and behavior (HES1 [50]), circadian functions (KLF15 [51], ZBTB14 [52]), neuronal identity (TCFL5 [53]), and mitochondrial biogenesis (NRF1 [54]).

Given that TF activity is modulated by intracellular signaling cascades (such as phosphorylation) responsible for responding and integrating external stimuli/perturbations, we performed kinase enrichment (KEA3 [55]) to map all the 79 unique TF proteins identified to the signaling pathways that might be driving the transcriptional activity changes and, ultimately, the changes in gene expression (**Figure 2c**, **Table S5**). We find that the top enriched kinases include JNK1/MAPK8, ERK1/MAPK3, ERK2/MAPK1, JNK2/MAPK9, P38D/MAPK13/SAPK4, JNK3/MAPK10, P38B/MAPK11, P38G/MAPK12/ERK6, and ABL. These results highlight the critical role of MAPK-signaling pathways in re-shaping the cortical transcriptional landscape during extended wakefulness.

Genetic diversity determines response to SD at the transcriptomic and chromatin accessibility levels

Previous work has shown that cortical gene expression and the effects of SD thereupon are under significant genetic influence, and thousands of quantitative trait loci (QTLs) have been associated with differences at the transcriptome level (expression - eQTLs) in the BXD population [16]. Indeed, some of the correlations between chromatin accessibility and transcript levels previously described are more dependent on clustering of BXD lines than on the SD effects (**Figure S2**). In agreement, dimensional reduction of the ATAC-seq data shows that regions with larger variance in accessibility within the entire dataset are more strongly associated with genetic background than with SD, a pattern which was similarly observed for the transcriptome (**Figure S3**). The effect of SD becomes noticeable only after considering lower variance regions, indicating that genetics is a major source of variability in chromatin accessibility and transcription levels, while SD has more modest, yet wider, effects at these molecular levels.

We leveraged the genomic data available for the BXD population [56] to further explore the connection between genetics and chromatin accessibility independently of the effect of SD. Similar to the effect of SD, we find genetic influences on chromatin accessibility (aQTLs) across the entire genome (**Figure S4a**), identifying 16'592 unique aQTLs (**Table S6**), corresponding to 15'566 regions (13'179 non-contiguous). Of the regions with accessibility statistically associated with genetic variants, 34% (5'273) are intronic, 34% (5'227) located to promoter regions, 22% (3'483) being in distal intergenic region, with 6% overlapping exonic regions (999). Likewise, cCREs were identified within 38% of the regions, of which 78% (5'267) were dELSs, 33% (2'223) matched CTCF binding regions (**Figure 3a**). Additionally, the genetic variants are mostly expected to act in *trans* (indirect), as only 5'675 regions (34%) are contained within the aQTL 95% confidence interval. Indeed, if *cis* (local) QTLs are considered as those having peak of the log of the odds ratio (LOD) within 10Kb of a region, we find that only 58 aQTLs, including 3 regions that have the LOD peak contained within the region itself. One of these 3 matches an enhancer signature 2-3Kb upstream of *Gpr37l1*'s TSS. Thus, genetic influence on chromatin accessibility seems to be due to effects on regulatory factors acting on the chromatin region, not local sequence variants. Regions with aQTLs are annotated to 7'038 unique genes, 1'293 of which also have a significant eQTL (38% of all transcripts with eQTLs), with 268 sharing the same LOD peak with a region annotated to it (**Figure 3b**). Of the 2'812 unique single nucleotide polymorphisms (SNPs) associated with aQTLs, a set of 1'357 unique SNPs (48%) are also associated with eQTLs, indicating that these variants underlie the shared genetic influence on chromatin accessibility and transcriptome.

We then considered if genetics and SD influenced chromatin accessibility at the same regions and, out of the 15'566 regions with an aQTLs identified, 1'219 regions (8%) are also significantly affected by SD. These regions are of particular interest as they represent a common interface between genetic and SD effects and, as such, might mediate the genetic contribution to variations in resilience or sensitivity to SD observed in the human population. To capture the genetic influence on the response to SD, we considered the statistical interaction between genetics and average effect of SD on chromatin accessibility for all regions (aQTLxSD). We find 24'836 aQTLxSD, corresponding to 23'376 regions and 3'135 SNPs. While 58% of aQTLxSD (14'285), resulted from one of the 2 alleles showing a lack of a significant response to SD (protected from SD), 40% (9'825) unexpectedly showed significantly opposed responses to SD for the 2 alleles (**Figure S4b**). We questioned if this behavior is also observed for interaction eQTLs (eQTLxSD) and, out of the 675 associations found, 388 (57%) show a protective effect while only 40 (6%) show opposite responses to SD, indicating that opposed responses to SD are proportionally less prevalent at the transcriptomic level. When comparing the accessibility and transcription, regions with aQTLxSD are annotated to 10'044 genes, of which 308 also have an eQTLxSD, corresponding to 46% of all eQTLxSD identified. In addition, 96% of the SNPs associated with an eQTLxSD are also associated with at least one aQTLxSD, indicating that most of the genetic influence on the transcriptomic response to SD also influences chromatin accessibility.

Integrative analyses of sleep highlight the decentralized genetic influence on the dense regulatory network of sleep response.

Our results confirm, and extend upon, the previous reports on the molecular effects of SD and genetics in the cortex at the level of gene expression (RNA-seq), chromatin accessibility (ATAC-seq),

transcriptional activity (footprint analysis), and intracellular signaling (kinase enrichment). These distinct molecular levels represent deeply connected layers of cellular regulatory networks that cannot be considered separately. In addition, sleep is known to have multiple distinct aspects which are under different molecular and genetic regulation 16,57. Accordingly, in our previous work we determined 341 sleep-related phenotypes based on EEG/EMG and locomotor activity recordings in the BXD panel, of median to high heritability, many of which showed significant association with genetic background (phenotypic - pQTLs) 16. To integrate all the available datasets for the BXD population, we derive two distinct sub-networks: one from the system genetics results (SG-sNet); and one from gene regulatory network inference (GR-sNet).

The SG-sNet was inferred by connecting chromatin regions, transcripts, TFs, and sleep phenotypes through their QTL association with genetic variants (SNPs) within the BXD population (Figure S5a). In addition, we connected all regions to the transcripts they are annotated to and those transcripts that shared the same LOD peak if their Pearson correlation test p-value was ≤ 0.05 (Figure S5b). The inferred SG-sNet (Table S7) allows us to explore genetic pathways associated with different sleep phenotypes, and their propagation from chromatin regions to transcript. This network contained 45’751 distinct molecular entities (nodes/vertices), most of which were chromatin regions (84%) with 8% transcripts, 8% SNPs, 0.2% sleep phenotypes, and 0.2% TFs. SG-sNet was divided into 1’225 non-connected components, the largest of which contained 36’253 nodes (79%), with the remaining components having less than 80 nodes each. Of all the components, 11 contained at least 1 pQTL association (edge/link), with 90% found on the largest component. To help interpret and compare the networks’ structures, we considered the graph-level centrality score for degree (the number of connections per node); closeness (shortest distance to all other nodes); and betweenness (the frequency with which an edge lies on the shortest path between all pairs of nodes). Focusing on the main connected component, this sub-network’s diameter is 38 (largest shortest path) with a mean distance between nodes of 12.6, and centralization values of 0.009 (degree), 0.09 (closeness) and 0.11 (betweeness). Degree distribution is highly skewed with 75% of nodes having 3 or less edges, while 1% (476) has more than 50 edges. The top 10 most connected nodes are the SNPs rs31443144, rs31666743, rs46476185, rs48042782, rs48295845, rs50057067; and the transcripts Hcn2, Hjurp, Mroh2a, and Pih1d2 (Figure 4a).

In addition to the BXD genetic information, the line-specific variations allowed us to infer regulatory relationships between chromatin states and transcription. We used GraNIE 58 to infer a GR-sNet using both ATAC-seq and RNA-seq signal for baseline and SD samples (Table S7). The inferred GR-sNet contained 6’868 distinct molecular entities, evenly split between chromatin regions (51%) and transcripts (48%) as expected, with 64 TFs predicted to drive the gene regulatory changes. This network was divided into 22 non-connected components, the largest of which contained 6’766 nodes (99%). In respect to the main connected component, its diameter is 14 with a mean distance between nodes of 3.8, and centralization values of 0.27 (degree), 0.3 (closeness) and 0.5 (betweeness), indicating a more centralized and clustered regulatory network when compared to the wider genetic effects described with the SG-sNet. Degree distribution is also highly skewed with 74% of nodes having 3 of less edges, and 4 nodes having more than 50 edges, corresponding to the TFs FOSB, FOSL2, JUNB, and NFE2L2 (Figure 4b). These results reveal a centralized regulatory response to SD, but a broader influenced by the genetic background on such response.

To obtain a global picture of SD regulation, we merged the SG- and GR-sNets, facilitating the assessment of the genetic influence on the regulatory elements (Figure S5c). In addition, we added the top enriched kinases identified in our enrichment analysis to their TF targets to integrate the layer of intercellular signaling into the network (Figure S5e,d). Evidence for TF binding to regions based on footprint analyses was also added to provide experimental support to the network connections (Figure S5e). To simplify the complex web of interactions, we filtered the network for transcript and chromatin regions significantly affected by SD and pruned any peripheral nodes (e.g. chromatin regions and TFs associated with only 1 other entity). To improve interpretability, the edges' naming was also simplified to reflect biologically meaningful relationships, rather than the method through which they were identified (Figure S5f). The final SD-response network (SD-Net) is divided into 994 components, the main one containing 9'267 (81%) nodes distributed as 43% transcripts, 34% chromosomal regions, 22% SNPs, 0.9% sleep phenotypes, 0.5% TFs and 0.1% kinases, with 34% of all edges originating from the GR-sNet, 32% from QTL associations, 19% from correlation analyses between chromatin accessibility and transcript levels, and 13% from footprint evidence. SD-Net shows that SD-related regulation of gene expression is clustered around early responding AP1 heretodimers acting as regulatory hubs with 2'522, 1'997, and 1'117 degrees for FOSL2, JUNB, and FOSB nodes, respectively, with FOSL2::JUNB (shared targets) coming fourth with 1'101 degrees, followed by the antioxidant TF NFE2L2 with a degree of 376. In addition, the SD-Net highlights clusters of sleep phenotypes, for example the genetic association between duration of seizures and REM sleep during SD 59 (Figure 4c), suggesting potential transcripts associated with these phenotypes such as Flnc, Gpr137c, Pacs2, Prox1, and Rab15. Though it does not provide mechanistic evidence that these genes are causally related to the sleep phenotypes, it nevertheless underlies their possible use as biomarkers. In addition, SD-Net also shows that closely related sleep phenotypes, like the SD-incurred loss of REM sleep and the resulting gain in REM sleep over the 24h of recovery are modulated by different genetic and molecular components.

Nrf1 regulates sleep pressure build-up, REM sleep and θ frequency

To further dissect which factors downstream of the centralized response to SD are important to sleep regulation, we focused on the TFs regulated by AP-1 factors, as these proteins represent downstream regulatory factors of the "branching response" to SD. Of the 5 TFs predicted to have their activity consistently affected by SD, HES1 and NRF1 were inferred to have direct regulatory connections to AP-1 factors such as FOSB, FOSL2::JUNB **(Figure S5)**. *Hes1* is an important mediator of the notch signaling, which has been implicated in sleep regulation [60], while *Nrf1* is a key factor in mitochondrial biogenesis [54]. Of these two factors, *Nrf1* is also affected at every molecular level examined: NRF1 is one the 5 TFs whose transcriptional activity is predicted to be decreased in all BXD lines after SD (**Figure 2b**), while its transcript is up-regulated by SD and, unlike *Hes1*, exhibits a sleep–wake-driven dynamics in the cortex [34]. The accessibility of the upstream dELS region (chr6:30,028,521-30,028,771), which contains a detectable FOSL2::JUNB footprint, is highly correlated with *Nrf1* expression (**Figure S2**). In addition to being correlated, both this region and the *Nrf1* transcript have overlapping a- and eQTLs (**Figure3c**), suggesting this region acts as a sleep-wake-driven enhancer.

Nrf1 (Nuclear Respiratory Factor 1, not to be confused with Nuclear Factor Erythroid 2 related factor-1) is a transcription factor involved in mitochondrial biogenesis, regulating the transcription of the mitochondrial transcription factor A (*Tfam* [61]), a pivotal player in mitochondrial DNA replication and

regulation, as well as several genes involved in oxidative phosphorylation, coordinating the bi-genomic regulation of mitochondrial function. Structural, size, and functional changes have been observed in neuronal mitochondria in response to SD; leading to transient mitochondrial dysfunction described during sleep recovery [62]. These observations have led to the hypothesis that mitochondrial function, energy metabolism, and/or reactive oxygen species (ROS) might be involved in regulating sleep [63,64]. In addition to its mitochondrial roles, *Nrf1* has also been shown to be involved in neuronal-specific functions such as neurite growth [65], and neurotransmission through regulation of the expression of the receptors *Grin1, Grin2b*, *Gria2*, and *Gabrb1* [66–68].

Given the results of our integrative analysis and *Nrf1*'s prominent role in mitochondrial and neuronal function, we decided to test the effect of *Nrf1* on sleep. However, the ubiquitous function of *Nrf1* means that a full knock-out (KO) of this gene is embryonic lethal [69]. To test the post-natal role of *Nrf1*, we acquired a new mouse line with insertion of LoxP sites flanking (flox) *Nrf1* exon 4 [70] (**Figure S6a**). We crossed these animals with *Camk2a*-CreERT2 animals to generate an inducible and conditional *Nrf1* mutant (icKO) affecting only *Camk2a* expressing cells. *Camk2a* is proposed to be a sleep-promoting kinase [26,71] mainly expressed in excitatory (glutamatergic) neurons [72], though its expression is not restricted to the cerebral cortex. We validated that treatment of *Camk2a*-CreERT2$^{Tg/0}$/*Nrf1*$^{flox/flox}$ animals with tamoxifen leads to the expected excision of exon 4 at the genomic and transcriptomic levels (**Figure S6b and S6c**). This genomic change leads to exon 4 being skipped in the final transcript and to a frame-shift in the open reading frame generating a premature stop codon (**Figure S6d**), which results in a truncated protein with disrupted secondary and tertiary structure (**Figure S6e**).

To test the impact of this deletion on sleep, we recorded EEG/EMG signals to quantify sleep-wake states of *Camk2a*-CreERT2$^{Tg/0}$/*Nrf1*$^{flox/flox}$ animals previously injected with tamoxifen (icKO) over 4 days, including 6-hours of SD starting on day 3 (light onset; ZT0-ZT6); and compared it to *Camk2a*-CreERT2$^{Tg/0}$/*Nrf1*$^{+/+}$ animals previously injected with tamoxifen (genotype control) and *Camk2a*-CreERT2$^{Tg/0}$*Nrf1*$^{flox/flox}$ animals previously injected with vehicle solution (tamoxifen control). Absence of *Nrf1* in *Camk2a*-expressing cells does not have a significant impact on time spent in NREM sleep or the NREM sleep recovery dynamics (**Figures 5e-g**). However, we did notice that, in *Nrf1*-ciKO animals, SD does not lead to the same high levels of normalized EEG delta(δ)-power (1-4 Hz) in NREM sleep after SD as in the two control groups (**Figures 5a and 5b**). Simulation analysis shows that these differences in δ-power could not be explained by eventual differences in the distribution of sleep-wake states [73] (**Figure S7a**). A lower average δ-power is also observed in the baseline dark period (active phase) and, though not significant when compared to both controls, indicates that the effects observed after SD do not result from the protocol used to keep mice awake (**Figure 5a**). Moreover, when awake, *Nrf1*-ciKO animals were not less active and did not spend less time in theta(θ)-dominated waking (TDW, **Figure S7b**), a waking stage associated with a faster build-up in δ-power [74]. These observations suggest that *Nrf1* plays a role in the kinetics of δ-power build-up during wakefulness, affecting mostly the activity in the fast δ-band (δ2 >2 Hz; **Figure 5c**). Increased δ-power is considered a marker for increased sleep pressure [75], in particular the dynamics of δ2 [76]. Accordingly, latency to sleep onset after SD was twice longer in *Nrf1*-icKO animals compared to the control groups (**Figure 5d**), confirming reduced sleep pressure after SD. Thus, *Nrf1* function in *Camk2a*-expressing neurons affects the dynamics of sleep pressure build-up, but not of NREM sleep time, suggesting these aspects of sleep homeostasis can be disentangled at the molecular level. While NREM sleep

time was not affected, baseline time spent in REM sleep was reduced by 24% (15min/12h) specifically in the light phase (**Figures 5e and 5f**). An effect on REM sleep recovery dynamics after SD was also observed, with the amount of REM sleep returning to the baseline levels earlier than in controls (within the first 18 hour of recovery), thus lacking the second day homeostatic 'negative rebound' in REM sleep time observed in the two control groups (**Figure 5g**). A comparison of the spectral composition of the EEG did not show major differences among the 3 groups for any of the sleep-wake states tested (**Figure S7c**). However, we find that the frequency of the θ-oscillation characteristic of TWD is reduced in *Nrf1*-ciKO animals (**Figure S7d**).

Lack of *Nrf1* in *Camk2a*-expressing cells led to detectable changes in the cortical transcriptome (**Figure S8a**). In unperturbed conditions, the *Nrf1*-ciKO affected 663 transcripts compared to genotype controls and 491 compared to tamoxifen controls, 356 consistent between the two control groups (**Table S9)**. Of these, 100 are up-regulated while 256 are down-regulated (**Figure 6a**). GO terms associated with these genes include the molecular function 'oxidized DNA binding' and the cellular component 'DNA repair complex'. Comparing to the findings in the BXD population, we find that 77% of the transcripts affected in *Nrf1*-ciKO were also affected by SD in the BXD population, with 47% being annotated to at least one DAR. In addition, 20% have an eQTL while 4% have an interaction eQTLxSD, thus suggesting that genetics influence the expression of some *Nrf1* targets, but not their response to SD. We then considered the effect of *Nrf1*-ciKO on the transcriptional changes in response to SD, and find that 883 transcripts were significantly affected only in these animals (**Figure S8b**), leading us to statistically test for significant interaction between *Nrf1*-ciKO and SD. Given statistical interaction requires higher powered studies, and in ciKO animals *Nrf1* function is only affected in a small proportion of cortical cells, we considered an uncorrected *p*-value <0.01 as supporting possible interaction between *Nrf1*-icKO mutation and SD transcript (**Figure 6b**). With this consideration, we find evidence for different response to SD in *Nrf1*-ciKO animals for 28 transcripts compared to the control animals, 5 of which were also affected in the baseline: the zinc finger proteins *Zfp329* and *Zfp575*, the ciliary complex subunit *Evc2*, the post-synaptic *Dlgap4* and the mitochondrial tRNA synthetase *Lars2* (**Figure S9**). Of these, only *Dlgap4* is differentially expressed in response to SD and has an eQTL association in the BXD population. We find no significant changes in the previously reported NRF1 targets *Grin1*, *Grin2b*, *Gria2*, and *Tfam*, suggesting these might be compensated once the new cortical steady state is established after the conditional mutation. We do find that the expression of the serotonin receptor *Htr1b* and ephrin receptor *Epha10* are affected (**Figure S9**), which might be relevant for the REM sleep phenotypes observed in *Nrf1*-icKO mice, as *Htr1b* has been implicated in the regulation of REM sleep [77].

Mitochondrial fission is not associated with sleep pressure build-up

Mitochondrial dynamics (fusion and fission) have been shown to change with time-spent asleep and awake and recent evidence suggests these processes might regulate sleep [35,36]. It is thus possible that the effect of *Nrf1* on the build-up of sleep pressure could be due to downstream changes in these dynamics. If such were the case, we would expect that interfering with mitochondrial fission or fusion would lead to similar phenotypes to those observed with *Nrf1*-icKO. To test this hypothesis, we re-analyzed our previous EEG/EMG data from a *Camka2*-driven icKO of dynamin 1 like (*Dnm1l*/*Drp1*) [78], a crucial protein that regulates mitochondrial fission and which has been implicated in sleep homeostasis in the fly, albeit with conflicting results [35,36]. Unlike *Nrf1*-ciKO, we do not observe any

difference in baseline or recovery sleep for *Dnm1l*-icKO compared to the controls (**Figure 7e and 7f**) and δ-power levels reached immediately after the end of SD did not differ (**Figures 7a and 7b**). We do, however, observe what appears to be a slower decay of δ-power during the subsequent 6h recovery sleep, which is not predicted from the observed distribution of sleep-wake [73] (**Figure S10a**). This observation led us to speculate that mitochondrial function affects δ-power decay-rate. Despite a trend of slightly higher rates, we found no significant changes in the rate of δ-power decay after SD in *Nrf1*-ciKO or *Dnm1l*-ciKO mice (**Figures 7c and 7g**). Similarly to *Nrf1*-ciKO, *Dnm1l*-ciKO shows a reduction in θ-frequency (**Figure S10d**), which co-occurs with a decreased trend of time spent in TDW and locomotor activity during the active dark periods (**Figure S10b**). These results suggest that mitochondrial dynamics in *Camk2a*-expressing cells modify θ-wave generation, but not sleep pressure, indicating multifaceted mitochondrial role on sleep and wake states. The lack of a sleep homeostatic phenotype in *Dnm1l*-ciKO animals suggests that mitochondrial fission is not an intermediate mechanism regulating *Nrf1* effect of sleep pressure. Instead, *Nrf1*'s role in sleep regulation could be due to changes in metabolic rate, ROS production [79] or, perhaps, neurotransmitter reception.

SD-Net highlights candidate genes mediating *Nrf1* sleep phenotypes

To understand what factors mediate the observed phenotypes downstream of *Nrf1*, we combined our transcriptional results from *Nrf1*-ciKO animals with the SD-Net to explore the downstream effects of *Nrf1*-ciKO at the molecular level and identify which factors might be involved in *Nrf1*'s regulation of sleep (**Figure 8a**). We identify 93 genes affected by *Nrf1* in the baseline present in SD-Net, including *Nrf1, Arc, Bhlhe40* and *Epha10*, and 8 genes with potential differential response to SD (interaction): *Anks6, Dlgap4, Etnk1, Evc2, Gmds, Ncoa5, Sde2*, and *Tubd1*; where *Evc2* (hedgehog signaling) and *Dlgap4* (postsynaptic guanylate kinase) are affected both in baseline and SD response.

To identify the most likely candidate genes mediating *Nrf1* role in sleep, we consider the shortest path between the transcripts affected in *Nrf1*-ciKO and the most relevant aspects of sleep present in the SD-Net, such as those related to NREM sleep time, θ-peak frequency and δ-power. We exclude any paths that crosses a TF, as these represent central regulatory hubs, connecting all branches of the SD-Net. We find that *Arc* is the nearest *Nrf1* target to the phenotypes related to θ-peak frequency in TDW (**Figure 8b**), having a regulatory connection to the upstream enhancer-like region chr15:74'622'118-74'622'618, which shares genetic variant *rs13481455* with the sleep phenotype. *Arc* is involved in neuronal plasticity, memory consolidation, and sleep homeostasis, and its transcription has been shown to be maximal in response to θ-bursts [80–83]. In addition, aspects of REM sleep in the baseline are related to *Aqp11*, an aquaporin that regulates oxidative H_2O_2 levels. This transcript is associated with a distal region chr7:98'463'563-98'464'313 and the variant *rs31920772*. A longer path is found for *Efcab5*, a calcium binding protein associated with epigenetic aging of the brain, and potentially with cognitive decline [84]. This transcript shares regulation with the nearby gene *Nsrp1* by the region chr11:76916623-76916824, where *Nsrp1*'s expression is related to REM gain on the second day of recovery from SD through a genetic variant locating to the Affy_10351506 probe (~chr1:170949421).

We did not find any transcript affected in *Nrf1*-ciKO mice near δ-power associated phenotypes present in SD-Net. However, we did notice that SD-Net places SD-induced changes in fast δ-power near θ-activity during wake, indicating a close genetic relationship between θ-power in waking (TDW) and

δ-power response during NREM sleep as previously proposed [74]. This observation suggests that the influence of *Nrf1* on δ-power and sleep-pressure build-up could be, not through direct transcriptional changes, but indirectly through changes to the neuronal state during TWD or, perhaps through changes at other molecular levels. Such indirect effects would still be expected to be detectable on the SD-Net, but not by looking at *Nrf1*-ciKO induced changes. As such, we searched SD-Net for transcripts associated with δ-power changes with SD and identify the transcripts *Rims4* and *Tc2n* are associated with the same SNP as changes in fast δ-power (rs49712246). *Tc2n* has been shown to regulate the activity of EGFR, ERK, STAT3, and FAK1 [85], while *Rims4* has been associated with presynaptic Ca^{2+} channels and neuronal arborization [86,87], a physiological process which has been associated with sleep pressure [3,88]. Though the pQTL is not detected in our BXD population [16], the variant rs13481905 has been previously associated with δ-power after SD in an older BXD set derived from a different D2 sub-strain [41,89] (**Figure 8c**). This SNP is present in SD-Net and associated to the calcium channel subunit *Cacng4* and to the acetylcholine receptor *Chrm4*. Muscarinic acetylcholine receptors have been implicated in regulating sleep architecture and REM sleep time [**90,91**], while *Cacng4* has been proposed to have strong AMPAR desensitization properties [**92**]. Given that *Chrm4* activity is regulated by Ca^{2+} [**93**], our results suggest that Ca^{2+} plays an important role in modulating the activity of proteins important for δ-power [94], with mitochondria being known to play an essential role in neuronal calcium Ca^{2+} buffering [95,96].

Discussion

In this work, we used the BXD genetic reference population to chart the molecular response of SD in the cerebral cortex. We initially focused on the unexplored epigenetic response to SD. Epigenetic modifications are thought to regulate gene expression through changes in accessibility of the chromatin, and thus we described these changes as a general readout of the epigenetic state of the cortex, as well as the "genetics of epigenetics", to complement our previous systems genetics dataset [16]. We then used two complementary approaches to infer a multiomics network representation (SD-Net) of the molecular changes induced by SD: a system genetics approach to understand how different molecular layers are genetically associated and the "genetic pathways of sleep"; and a regulatory inference approach to integrate the multiomics information into the "regulatory pathways of sleep". SD-Net represents an initial resource to explore the molecular responses to SD and generate data-driven hypotheses regarding the regulation of sleep. We exemplify the use of this resource in 3 different ways: 1) Identification of candidate biomarkers: we identify a genetic relationship between duration of seizures and REM sleep during SD, these aspects of sleep being associated with the genes *Flnc*, *Gpr137c*, *Pacs2*, *Prox1*, and *Rab15*; 2) Identification of candidate sleep regulators: we identify *Nrf1* as an transcription factor involved in sleep pressure build-up. In addition, SD-Net allows us to identify a putative sleep-enhancer though which *Nrf1* is regulated by the core AP-1 factors involved in the early response to SD; and 3) Integration of new results: we query the SD-Net to identify genes affected in *Nrf1*-ciKO animals, such as *Arc*, *Aqp11*, and *Efcab5*, which are closely associated with the phenotypes observed in these animals.

Sleep-wake states and chromatin accessibility in the cerebral cortex

Similar to what has been reported for transcription, we find that SD significantly impacts chromatin accessibility across the entire genome. The majority of the genomic regions affected are non-coding,

regulatory regions, which become more accessible after SD. Decreases in accessibility associate with CTCF signatures, a protein known not only for insulating topologically-associating DNA domains, but also for mediated promoter contacts with long-range enhancers through establishment of chromatin loops [38,97]. This suggests that higher dimensional chromatin conformation changes underlie the response to SD. In addition, CTCF has been implicated in neuronal development and behavior [98], indicating that these processes are indeed relevant for neuronal function. Although these changes in accessibility do not necessarily translate into changes at the transcriptional level, they do reflect an important step in the epigenetic regulation of gene expression [99]. We find evidence that the effects of SD on chromatin accessibility are at least partially correlated with the expression of genes associated with synapse organization and activity, hormonal response, and memory. This includes a number of immediately early genes (IEG), implying that chromatin accessibility changes occur quickly in response to SD.

We estimated transcription factor (TF) activity from the changes in chromatin accessibility, and identified AP-1 complexes as TFs with higher binding affinity after SD, which is consistent with their role as IEGs. However, the most consistent activity changes across the BXD panel were for TFs which are predicted to have an overall decrease in binding after SD. Transcription activity is commonly modulated by intracellular signaling processes such as phosphorylation by kinases, which are prime pharmacological targets for therapy development. Enrichment for kinase targets highlights critical role of MAPK signaling pathways in re-shaping the cortical transcriptional landscape during extended wake, particularly through JNK1-3, which phosphorylate JUN proteins, one of the subunits of the AP-1 heterodimer; and ERK2, which has been proposed to promote sleep [100]. From these results, we conclude that neuronal activity during extended wake initiates MAPK signaling cascades, which lead to the early activation of AP-1 factors which, as pioneers factors, are able to open the cortical chromatin [101]. However, it is important to note that the enrichment was limited to identifying kinases targeting the identified TFs, and thus would not be able to identify other kinases which are not known to directly target TFs, but might still influence sleep, as is the case of SIK3 [102,103] .

Genetics of the molecular SD response

Despite the extensive changes induced by SD on the epigenetic landscape of the cortex, genetic variants across the BXD population were associated with larger variance in both chromatin accessibility and transcription levels. This could be due to the fact that genetic variation impacts all cell types in a stable, non-reversible manner, while environmental perturbations, such as SD, are instead more likely to transiently affect subpopulations of cortical cells differently, thereby having, on average, a smaller effect at the tissue level at which we quantified these changes. It would thus be of interest to assess in follow-up work whether SD has, relatively to genetic-background effects, larger effects in some cell types than in others. Regardless, we find that as many as 1’357 genomic variants (SNPs) alter chromatin accessibility in the cortex and simultaneously influence the expression of at least 1’293 genes. The effect of these SNPs seems to be mostly indirectly by affecting DNA interacting factors (in *trans*) instead of directly through sequence changes (in *cis*). Given these SNPs act *in trans*, these observations suggest that the genetic variation impacts the binding of some other factor (*e.g.* TFs) to these regions, indirectly modulating the expression of these genes.

Of particular interest are the molecular responses to SD that varied according to genetic background (interaction e- and aQTLs), as these might relate to the inter-individual difference in the resilience to sleep loss. This genetic influence on the response to SD is often shared among molecular layers, with 49% of interaction eQTLs being also identified for the interaction aQTLs for the accessibility of nearby chromatin regions. This suggests underlying genetic pathways of sleep, where a genetic variant alters gene expression by modifying transcriptional activity through changes in chromatin accessibility. The influence of genetic variants on the response to SD ranges from decreased (protected) responses in 58% of the interaction aQTLs identified, to being associated with opposite responses in 40% of the cases. Such striking effects where depending on carrying a B6 versus a D2 allele at the aQTL closes or opens the chromatin in response to SD, are less prevalent at the level of transcription, being noticeable in only 6% of interaction eQTLs. As most preclinical research relies on the use of a single mouse line (B6), our results from the BXD population underscore the importance of using more than one genetic background when studying the molecular consequences of an environmental challenge, or, as in our case, aiming at identifying core molecular mechanisms that are not strain dependent.

Genetic and regulatory network of SD response

Independent analyses of different molecular levels can provide a snapshot description of what changes occur during SD. However, to obtain a more global appreciation of how these changes relate and which pathways partake in the cortical response to SD, a full multi-omics integration is required. As such, we integrated the genomic, chromatin accessibility, transcriptomic, and phenotypical data collected so far in the BXD population, and inferred a regulatory network (SD-Net) based on two distinct approaches: system genetic associations and gene-regulatory correlations. SD-Net models the underlying response to SD in the cortex, highlighting the centrality and MAPK (JNK, ERK, p38) pathways in activating AP-1 complexes (FOSL2, FOSB and JUND), which is consistent with a role for phosphorylation cascades on sleep [26]. The centrality of these factors also suggest that the molecular effects of SD are causally linked to increased sustained neuronal activity. In contrast to the centralized molecular regulation, the associations with genetic variants (QTLs) are spread out in the peripheral branches of the network, leading to distinct aspect of sleep. As such, the inferred SD-Net illustrates how one central point of regulation can lead to differentially affected aspect of sleep, and how distinct genetic variants can affect these sleep phenotypes independently.

It is interesting to note that changes in the transcriptional activity of AP-1 factors are not consistently significant in every BXD strain, and yet are inferred to be central regulatory nodes and key neuronal effectors. We speculate that such central genes in neuronal activity are under strong selective pressure, which also could help explain why we observe nearly no eQTLs associated with these genes. Given their centrality however, small changes in AP-1 response to neuronal stimulation might be associated with vast phenotypical changes in sleep by propagating its effect downstream the regulatory network, explaining inter-individual differences in sleep resilience. One interesting example is *Fosb* truncated isoform *ΔfosB*, which was found to be extremely stable, leading to long term-effects in addiction and reward systems [104], both associated with decreased sleep time [105,106]. In addition, elevated levels of ΔfosB [107] lead to increases in brain-derived neurotrophic factor (*Bdnf*) levels [108], which have been associated with the build-up of sleep pressure [109], thus suggesting an unexplored link between the

regulation of the expression of the early response factors such as *Fosb*, and the long-term effects of SD.

Mitochondria and the need for sleep

SD-Net identified a number of candidate transcripts involved in the response to SD, such as *Hcn2*, *Hes1*, and *Nrf1*, where the pacemaker ion channel *Hcn2* and the notch-signaling factor *Hes1* have been linked to aspects of sleep [60,110]. Given the role of *Nrf1* in mitochondrial biogenesis but its unknown impact on sleep, we tested *Nrf1*'s loss of function in *Camk2a* expressing cells. Skipping *Nrf1* exon 4 in these cells led to changes in the dynamics of δ-power build-up and reduced sleep pressure after SD, but no significant changes in NREM sleep. On the other hand, REM sleep time in the baseline and gain during recovery are affected in *Nrf1*-ciKO mice. Unexpectedly, we find that *Dnm1l*-icKO in *Camk2a* expressing cells has only a small effect on sleep unlike previously reported in *D. melanogaster* [35,36], albeit with contradictory results even in that model organism. This lack of genetic evidence suggests that the role of *Dnm1l* in sleep regulation, if evolutionary conserved, might be through non-*Camk2a* expressing cells, which leads us to believe that mitochondrial fusion and fission dynamics are not related to the observed *Nrf1* phenotypes, except perhaps changes in θ-activity during TDW. This stage of waking, and associated θ-power, has been associated with cognition and memory [5], processes which have been previously reported to be affected in *Dnm1l*-icKO animals [78]. As such it is possible that *Nrf1*-icKO animals are also affected by mild cognitive dysfunction, though we did not test this. Importantly, we were able to query SD-Net and identify *Arc*, *Aqp11*, and *Efcab5* as downstream targets of *Nrf1* and as strong candidate genes affecting the frequency of θ-activity during TDW and REM sleep time in baseline and recovery.

Even though we have not tested for full genetic epistasis to exclude that *Dnm1l* and *Nrf1* function in the same genetic pathway, our results suggest that *Nrf1* might instead indirectly regulate sleep pressure through its mitochondrial biogenesis function (increase in mitochondrial protein/DNA mass) and subsequent changes in oxidative metabolism rate and/or ROS production [79,111]. SD-Net does not capture such non-transcriptional effects and thus it would be essential to study the genetics and response to SD of additional molecular layers, in particular at the level of proteins and their translational modifications [25]. We predict that such indirect effects could be related to the mitochondrial Ca^{2+} buffering role and the modulation of genes such as *Rims4* [86,87], *Chrm4*, *Cacng4* [92]. Alternatively, *Nrf1* function in sleep regulation might be through direct or indirect effects on neuronal function and/or plasticity [65], particularly through genes such as *Htr1b* [77], *Epha10* [112] or *Dlgap4* [113].

Conclusion

Based on our multi-omics analyses, we propose a model where neuronal activity induces MAKP signaling cascades leading to the increase of AP-1 activity, coordinating the central regulatory response to SD. In turn, this induces epigenetic and chromatin structure changes, regulating accessibility of genomic regions, such as the "wake-driven" distal enhancer-like region correlated with *Nrf1* transcript levels, which we demonstrate is a gene involved in sleep-pressure build-up. *Nrf1* is a key mitochondrial biogenesis, likely influencing sleep by modulating the activity of ions channels [28–30] through intracellular oxidative status [79,111] and the availability of Ca^{2+} signaling and downstream phosphorylation cascades [26,94]. Our results thus point to the involvement of a molecular network of

“sleep homeostats”, instead of a single molecule or pathway, with mitochondrial function as important intermediate providing a unifying framework for distinct molecular hypotheses sleep regulation.

Figures

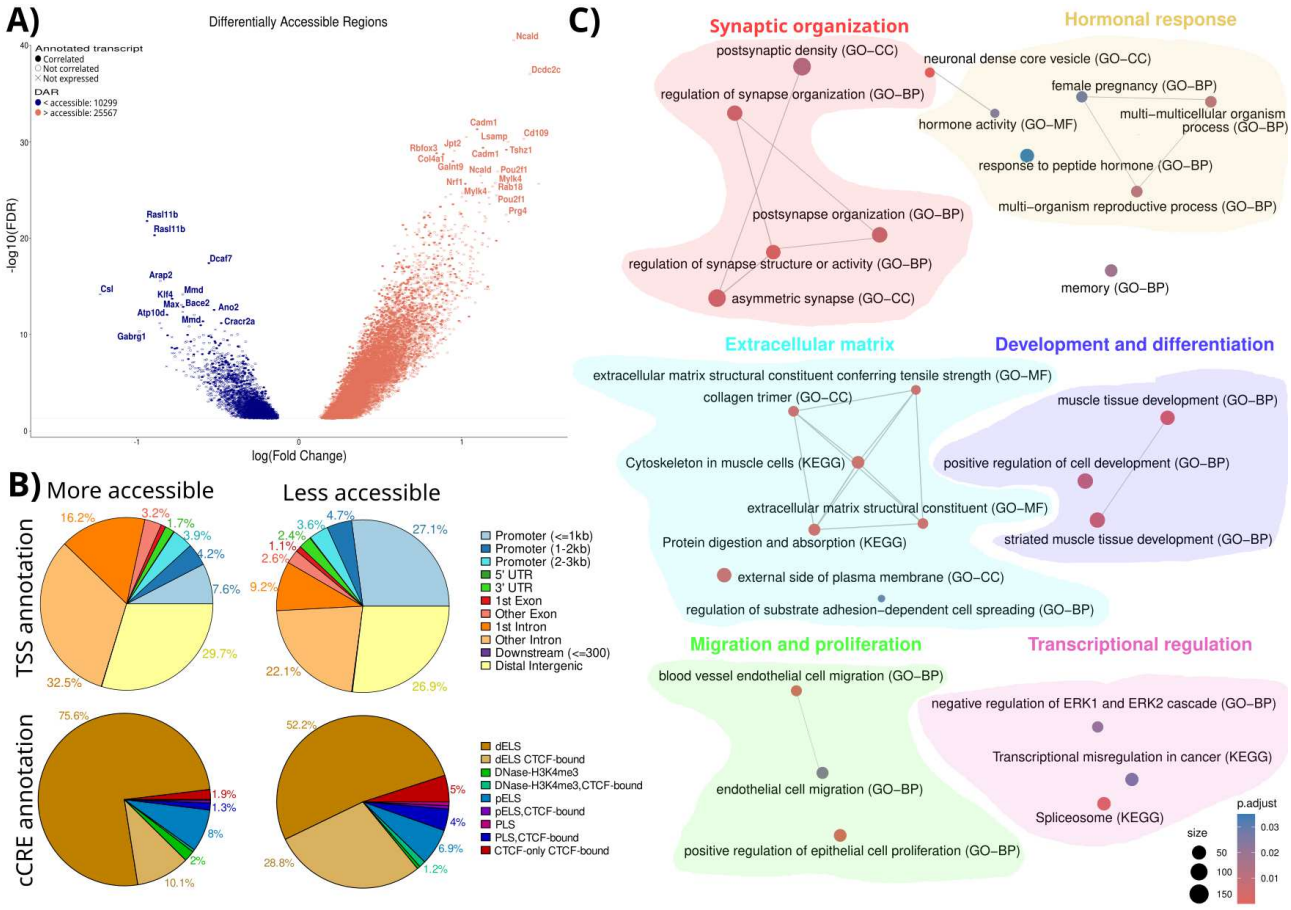


Figure 1: Acute sleep deprivation leads to genome wide changes in chromatin accessibility

a) Volcano plot showing the identified 35’866 differentially accessible regions (DAR), of which 10’299 (28%) were less accessible (blue), 25’567 (71%) more accessible (red) after SD. The most statistically significant regions are annotated to the closest transcription starting site (TSS) for easier interpretation and readability, which means that multiple points (regions) can map to the same gene. *Filled dots*: regions with significant correlation to the annotated transcript after multiple test adjustment; *Open dots*: regions without significant correlation to annotated gene; *x*: regions annotated to genes filtered out due to low counts from RNA-seq data or without annotated gene. **b)** Distribution of regions more (left) or less (right) accessible after SD based on their distance to TSS (top) or on the ENCODE candidate cis-regulatory elements (cCRE) database (bottom). *PLS* (promoter-like signatures) fall within 200 bp of an annotated TSS. *ELS* (enhancer-like signatures) within 2 kb of a TSS are denoted proximal (pELS), while the remaining subset is denoted distal (dELS). *UTR*: untranslated regulatory region of the coding sequence. **c)** Enrichment map (emap) for GO terms and KEGG pathways associated with the identified DARs. Genomic regions were annotated to their nearest gene and only transcripts considered for differential expression analysis (passing low expression filter for RNA-seq) were used as background reference, thus excluding genes not expressed in the cortex. In addition, the results were filtered to contain terms also enriched for differential gene expression. Size is proportional to the number of genes matching the enriched term, and color to the enrichment *p*-value. Relationship (shared genes) between enrichment terms are shown by the edges connecting the terms, which were manually grouped for easier interpretation.

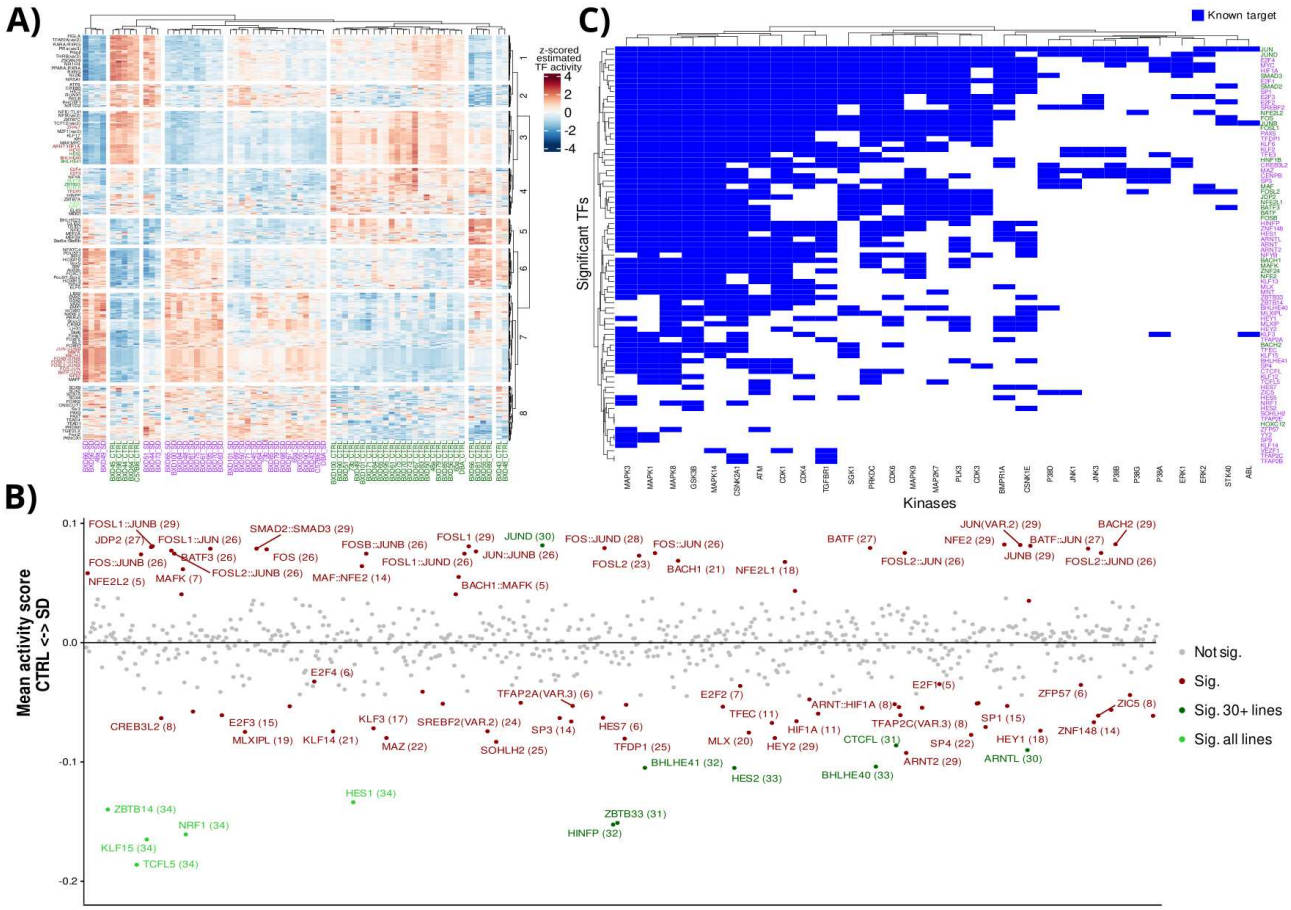


Figure 2: Transcriptional and signaling changes upstream of the chromatin-accessibility changes.

a) Heatmap of the z-scored transcriptional activity for each BXD line and treatment combination, estimated from footprint accessibility in DARs for transcription factors (TFs) with known binding motif. Control (green, CTRL) and SD (purple) samples separate into distinct groups, driven by TF activity on clusters 3, 4 and 7. Some line specific differences are also observed, in particular 3 baseline CTRL groups distinguishable by activity of clusters 1, 2, 5 and 6. SD samples are also separated into 4 main clusters defined by high or low activity in clusters 6 and 7. *Blue* and *Red*: Below and above mean estimated transcriptional activity, respectively. **b)** Aggregated estimation of the transcriptional activity changes for all TFs after SD. Meta analysis across all BXD lines was used to identify TFs with significant changes in predicted activity after SD (red). The 13 most consistently affected TFs are shown in green (significant in >30 BXD lines), with the 5 significantly affected in all lines shown in lighter green. **c)** Binary heatmap of TFs known to be downstream targets of the most enriched kinases. Blue lines mark known phosphorylation targets. TFs with predicted increase in activity after SD are shown in green, and those with predicted decrease in activity are shown in purple.

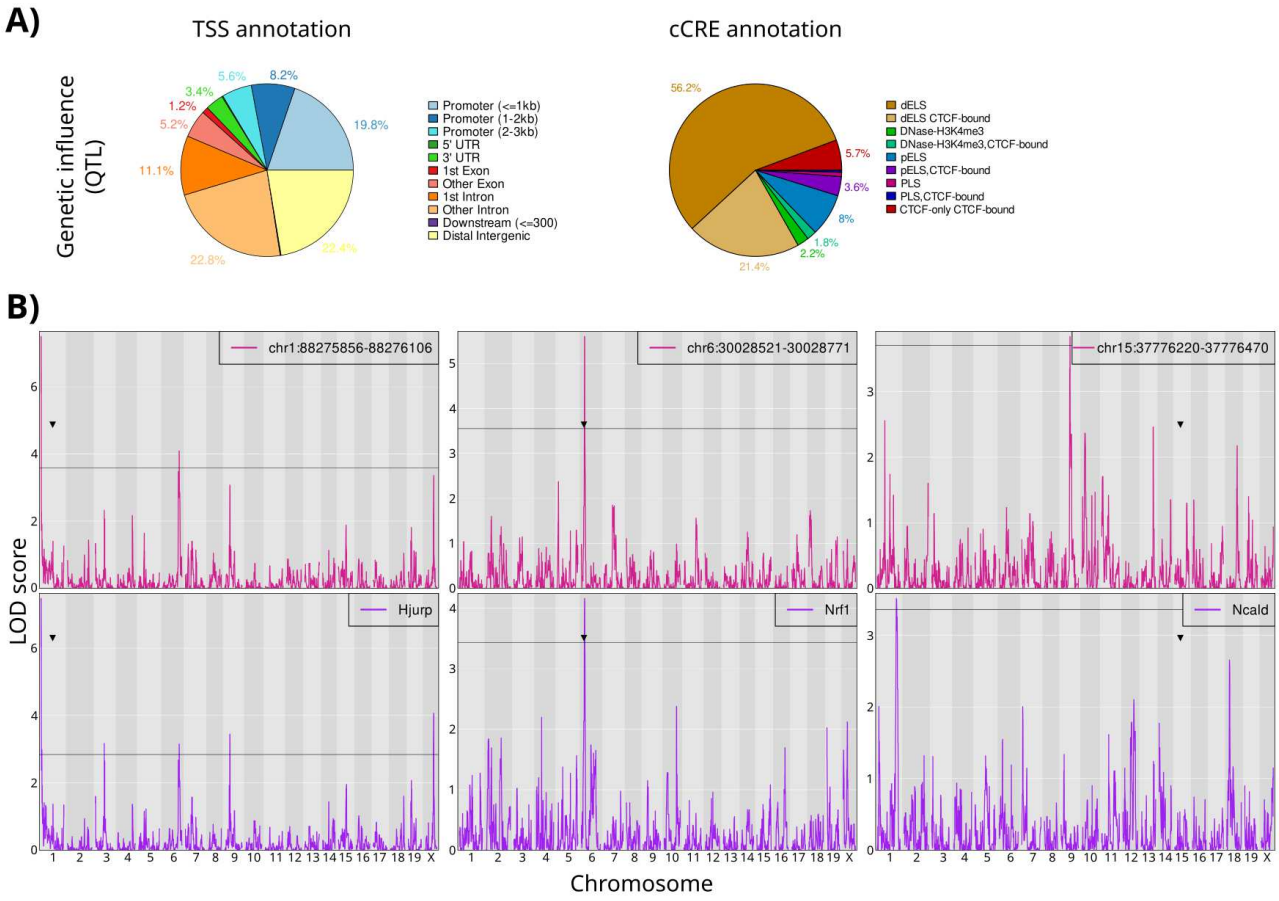


Figure 3: Genetic influence on chromatin accessibility and transcriptome.

a) Distribution of aQTLs based on their distance to transcription starting sites (TSS; left) or based the ENCODE candidate cis-regulatory elements database (cCRE; right). *PLS* (promoter-like signatures) fall within 200 bp of an annotated TSS. *ELS* (enhancer-like signatures) within 2 kb of a TSS are denoted proximal (pELS), while the remaining subset is denoted distal (dELS). *UTR*: untranslated regulatory region of the coding sequence. **b)** Examples of aQTL (magenta, upper panels) and associated eQTL (purple, lower panels). *Hjurp* shows an exact match in the SNP associated with the maximum LOD score for a- and eQTL on chromosome 1; *Nrf1* and *Hjurp* shows a closely located aQTL and eQTL peak on chromosome 6; and *Ncald* illustrates a case where the aQTL (chromosome 9) and eQTL (chromosome 1) are not shared. Approximate location of gene and regions on the genome are shown by the black triangles.

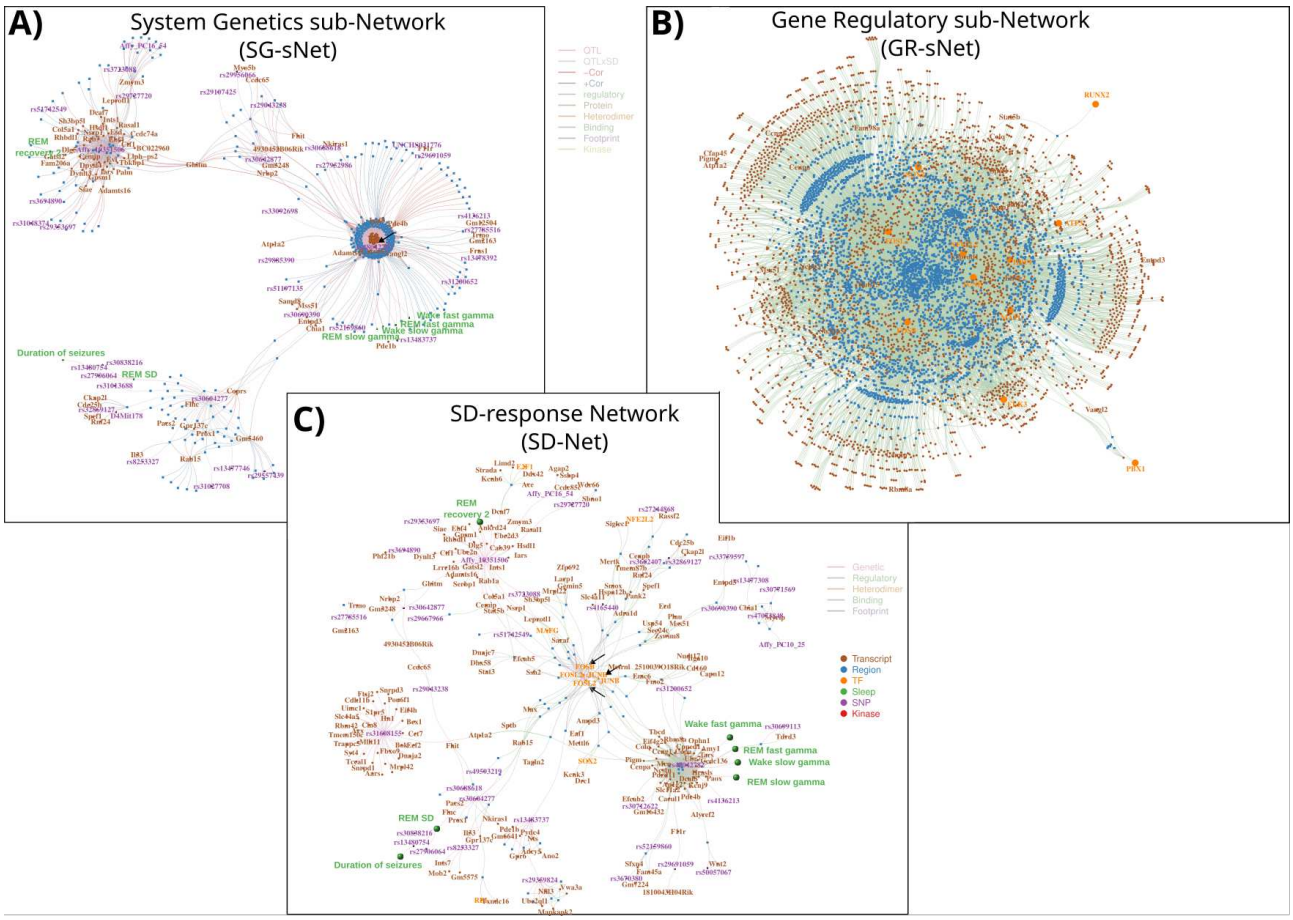


Figure 4: Integrative network of the SD response.

a) Detail of the systems genetics sub-network (SG-sNet) illustrating the complex interconnection of genetic effects on the cortical molecular levels in the baseline (QTL) or in response to SD (QTLxSD). Regions and genes are connected if they show significant correlation between accessibility and transcript levels. **b)** Gene regulatory sub-network (GR-sNet), illustrating the predicted binding of transcription factors (TFs) to chromatin regions, and from changes in accessibility to transcript levels. This regulatory network is highly centralized around FOSL2, FOSB and JUNB. All TFs in the network, and transcripts in the SG-sNet are highlighted for reference. **c)** SD-Net integrating both system genetics and regulatory networks (see Figure S5 for more information). SD-Net illustrates the core regulatory center of the response to SD, with decentralized genetic effects on peripheral branches of the network. The represented networks are an illustration of a subset of the entire SD-Net. Blue: Chromatin regions; brown: transcripts; orange: transcription factors; purple: SNPs; red: kinases; green: sleep phenotypes. Note that edges of SD-Net (bottom) are not the same as those of the SG- and GR-sNets (top). Arrows point to high degree nodes (>50 connections). More details on Table S6.

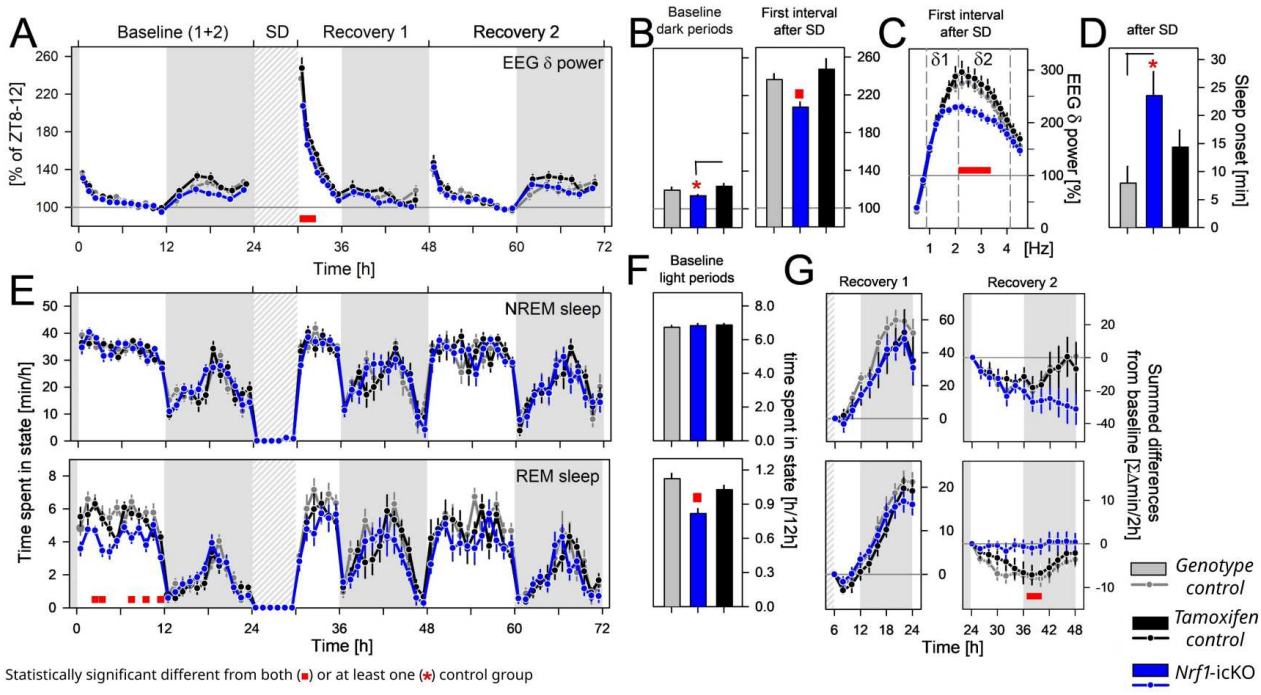


Figure 5: Inducible knockout of *Nrf1* in *Camk2a* expressing cells impacts sleep pressure and REM sleep recovery.

a) EEG δ-power during NREM sleep over the course of the 4-day experiment. After SD (30h), δ-power levels reached are significantly lower in *Nrf1*-icKO animals than for animals of both control groups. Note that the 2 baseline days are averaged into one. **b)** Quantification of δ-power in the baseline dark periods (left) and after the SD (right panel) show lower average levels compared to both control groups. **c)** Spectral decomposition of relative EEG changes in the δ-band (1-4 Hz) during NREM sleep in the first recovery interval show that significant changes are limited to the 'fast' or δ2 (2.25-4.0Hz) band. **d)** Sleep-onset latency after SD is longer in *Nrf1*-icKO animals compared to controls. **e)** Hourly values of average time spent in NREM (upper) and REM (lower panel) sleep over the course of the 4-day experiment. Note that *Nrf1*-icKO animals spent less time in REM sleep in the baseline light periods. **f)** Quantification of time spent in NREM and REM sleep in the baseline 12h-light periods. **g)** Daily accumulated differences of NREM and REM sleep compared to the baseline sleep during recovery after SD (recovery 1; time 30-48h) and the day after (recovery 2; time 48-72h). Distinct REM sleep recovery dynamics are noticeable for *Nrf1*-icKO animals during recovery day 2. *Gray*: *Camk2a*-CreERT2$^{Tg/0}$*Nrf1*$^{+/+}$ animals treated with tamoxifen (Genotype control); *black*: *Camk2a*-CreERT2$^{Tg/0}$*Nrf1*$^{flox/flox}$ animals treated with vehicle solution (Tamoxifen control); *blue*: *Camk2a-CreERT2*$^{Tg/0}$*Nrf1*$^{flox/flox}$ animals treated with tamoxifen (induced and conditional knock-out – icKO). Hourly statistics for for time course panels (a and c) are only shown when icKO differed from both controls (no red asterisks), to prevent figure overcrowding.

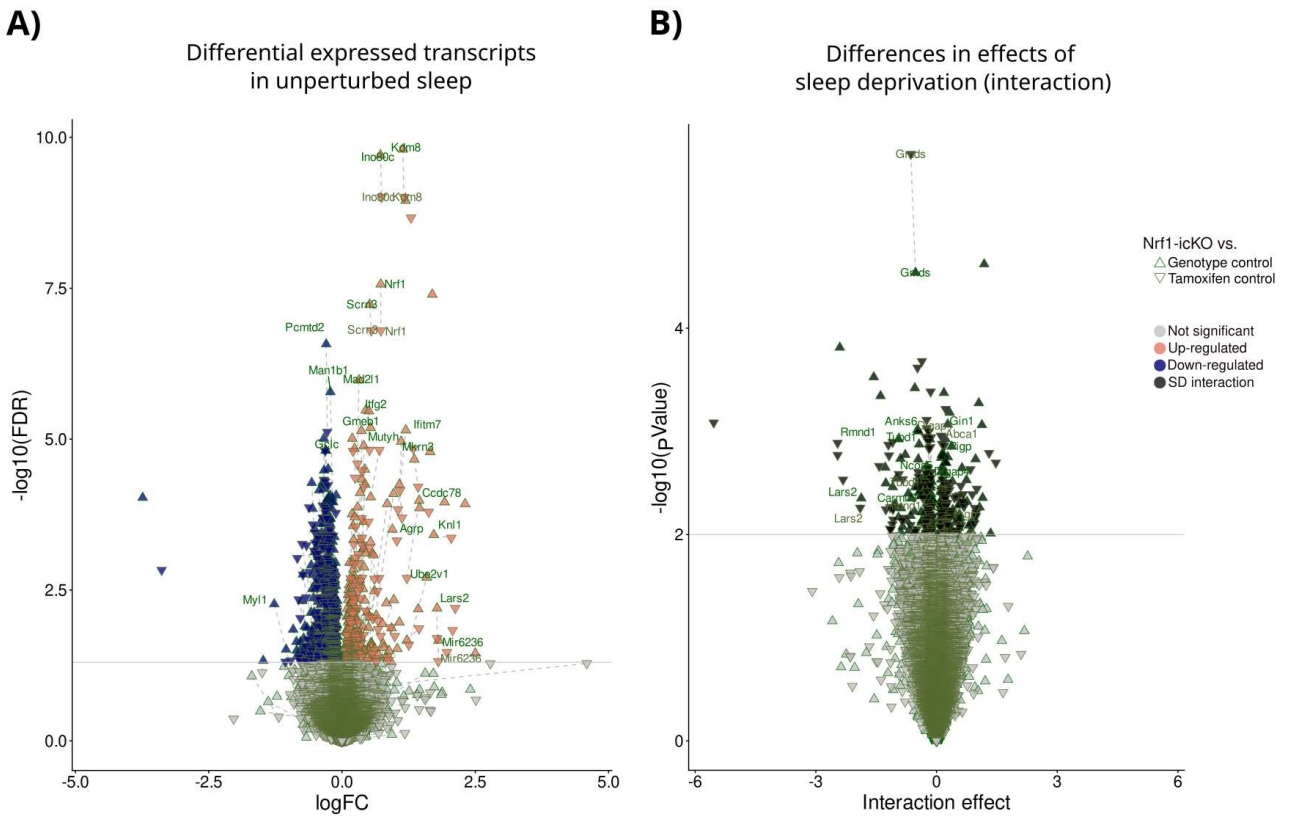


Figure 6: Transcriptomic changes in the cerebral cortex induced by mutation of *Nrf1* in *Camk2a*-expressing cells.

a) Volcano plot for the cortical transcriptional differences in undisturbed sleep conditions (baseline, ZT6) between *Nrf1*-icKO and each control group (genotype and tamoxifen) using a statistical cut-off of FDR < 0.05. **b)** Volcano plot for the differences in the SD response using non-corrected statistical cut-off of *p*-value < 0.01, to identify transcripts changing response to SD in *Nrf1*-icKO animals compared to both control groups. *Upwards triangle*: Differential expression compared to genotype control; *Downwards triangle*: Differential expression compared to tamoxifen control. *Blue*: down-regulated genes in the baseline. *Red*: up-regulated genes in the baseline. *Black*: genes with significant changes in response to SD (statistical interaction). *Gray*: non-significant genes. Since two comparisons are shown, the same genes are connected by a dashed gray line to highlight similarities between differences to both controls.

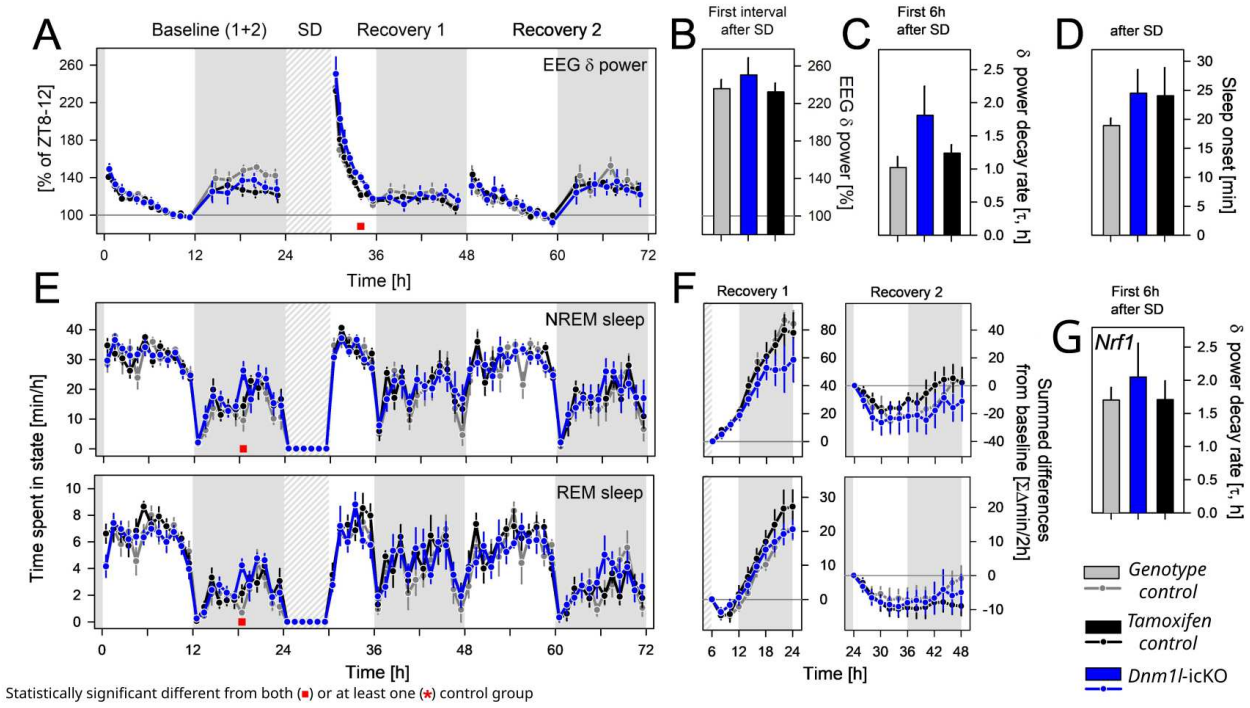


Figure 7: Inducible knockout of *Dnm1l* in *Camk2a*-expressing cells does not show similar phenotypes to *Nrf1 knockout.*

a) EEG δ-power in NREM sleep over the course of the 4-day experiment. After SD (30h), δ-power does not consistently differ between *Dnm1l*-icKO and control animals **b)** Quantification of δ-power after the SD showing no overall significant difference to both controls. **c)** Estimation of δ-power decay shows *Dnm1l*-icKO do not have lower decay rates as hypothesized from the shape of the curve in a). **d)** No significant differences are found in sleep latency onset immediately after SD between *Dnm1l*-icKO and controls. **e)** No significant changes in average time spend in NREM and REM sleep over the course of the 4 days of experiment are found between *Dnm1l*-icKO and controls. **f)** Daily accumulated differences of NREM and REM sleep compared to the baseline sleep during recovery after SD (recovery 1; time 30-48h) and the day after (recovery 2; time 48-72h) do not differ between *Dnm1l*-icKO and controls. **g)** Estimation of δ-power decay for *Nrf1*-icKO is also not statistically different from that of the controls. *gray*: *Camk2a*-CreERT2$^{Tg/0}$*Nrf1*$^{+/+}$ animals treated with tamoxifen (Genotype control); *black*: *Camk2a*-CreERT2$^{Tg/0}$*Nrf1*$^{flox/flox}$ animals treated with vehicle solution (Tamoxifen control); *blue*: *Camk2a-CreERT2*$^{Tg/0}$*Nrf1*$^{flox/flox}$ animals treated with tamoxifen (induced and conditional knock-out - icKO). Hourly statistics for for time course panels (a and c) are only shown when icKO differed from both controls (no red asterisks), to prevent figure overcrowding. Compare results to Figure 5.

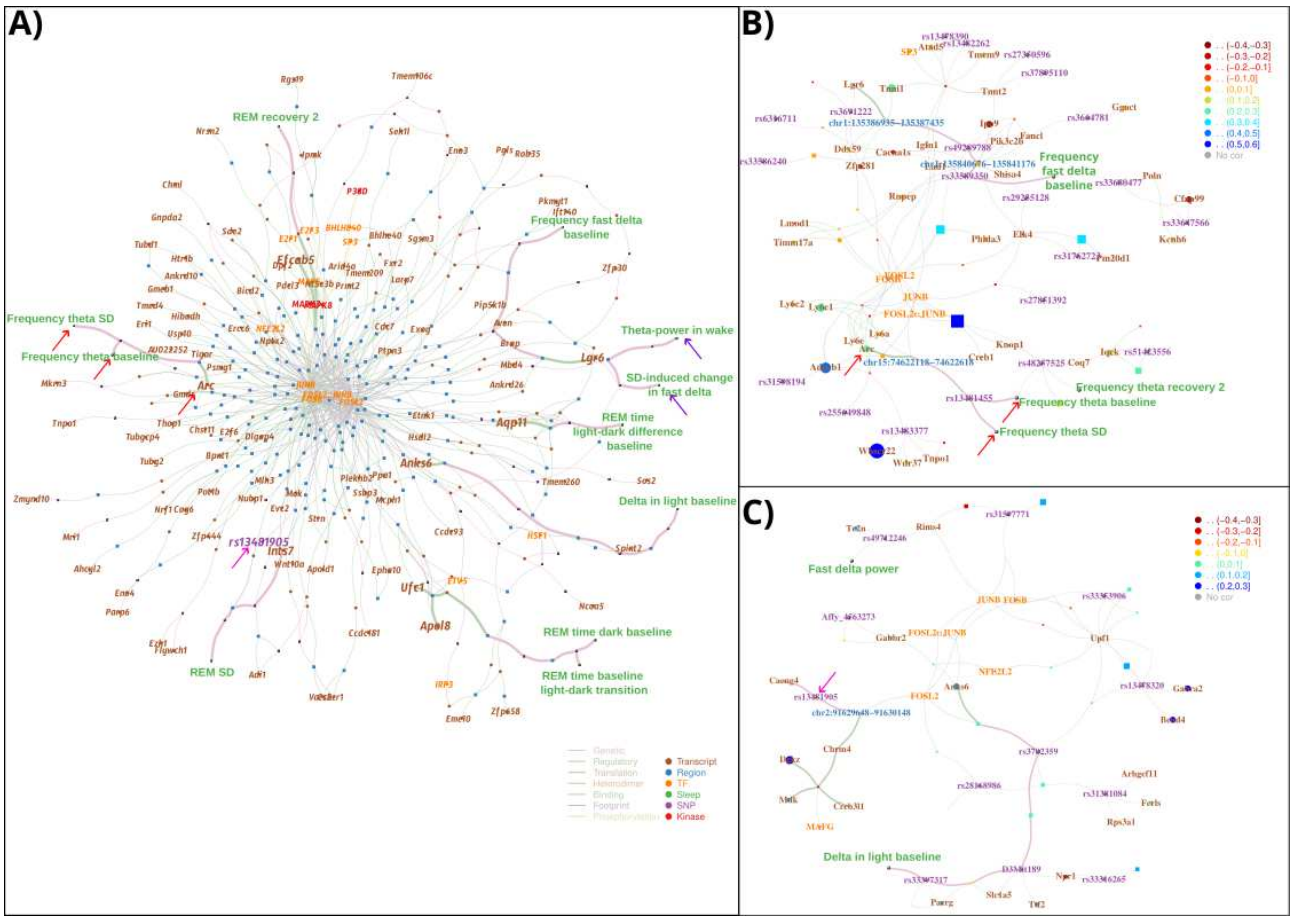


Figure 8: Integrative network identifies *Nrf1* candidate targets associated with affected sleep phenotypes

a) Detail of the systems genetics subnetwork (SG-sNet) illustrating the location of the transcripts that are affected in Nrf1-icKO mice and their relationship to the EEG phenotypes δ- and θ-activity, previously descripted in the BXD population 16. All transcripts shown are affected in Nrf1-icKO in either undisturbed conditions or respond differently to SD. Transcription factors (TFs), kinases, and the rs13481905 SNP are labeled as well, for reference. Red arrows show location of Arc matching panel b); Pink arrow shows location of rs13481905 matching panel c); Purple arrow show closely associated θ- and δ-activit phenotypes. **b)** Highlight of the network for the sleep aspects related with θ-activity, showing genetic proximity of Arc to θ-frequency. Nodes are colored by correlation between the transcript levels and the average value for the θ-related phenotypes, and the names of regions were removed for clarity. **c)** Highlight of the network for δ-power showing transcripts associated with fast δ2 power and the previously identified SNP related to δ-power levels after SD (rs13481905 41); is also found in the network. Nodes are colored by correlation between the transcript levels and the average value for the δ-related phenotypes, and the names of regions were removed for clarity. Sleep phenotype names have been simplified for interpretations. More details on Table S6.

Supplementary Figures

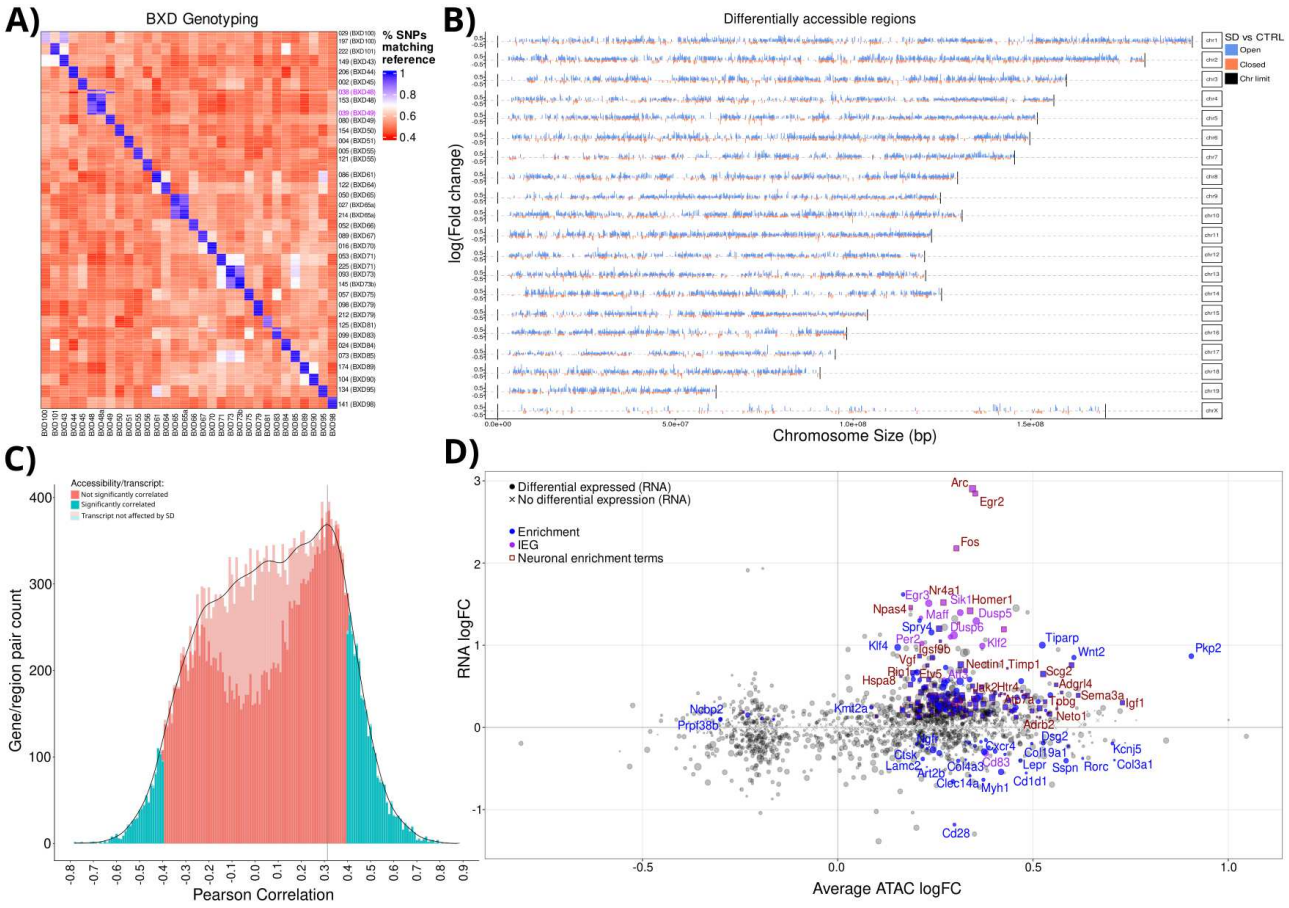


Figure S1: a) Validation of the BXD-line identity of the samples by variant calling of identified regions. Columns correspond to reference genotype and rows to the experimental samples, both ordered by line number to generate a clear diagonal line. Color gradient indicates the percentage of single nucleotide polymorphisms (SNPs) that match the reference sequences (blue=100%; white=70%; red=40%). Clustering of percentage of variants matching the reference genotypes identifies that two samples have been mislabeled (038 and 039; purple). The BXD lines ID for these 2 samples were corrected to match the experimentally observed genotype. **b)** Distribution of differentially accessible regions (DARs) throughout the genome shows widespread changes without any clear pattern. Chromosomes are displayed individually and their boundaries shown by black lines, with the relative location of regions with statistically significant changes in accessibility (FDR < 0.05) shown in blue for more accessible regions ($\log_2$FC > 0) and red for less accessible regions ($\log_2$FC <0). **c)** Distribution of Pearson ρ correlation coefficients between each identified DAR and the level of the transcript it was annotated to. The correlation distribution is skewed towards positive correlations, with a mode around ρ=0.3 (vertical line). *Red*: non-significantly correlated pairs; *blue*: significantly correlated pairs (adjusted *p*-value < 0.05). Transcripts that were not significantly differentially expressed after SD are shown in transparent color. **d)** Correlation of the average $\log_2$FC response to SD for the identified DARs and the expression of their annotated gene. Since many regions might be annotated to the same gene, the average accessibility response was considered. Transcripts are shown as dots if significantly affected by SD, and as X if not. Genes associated with enriched terms or functions are shown in blue. Immediate early genes (IEGs), which are expected to quickly respond to SD, are shown in purple. Genes associated with enriched terms for neuronal functions in both RNA-seq and ATAC-seq data are shown as squares with brown contour.

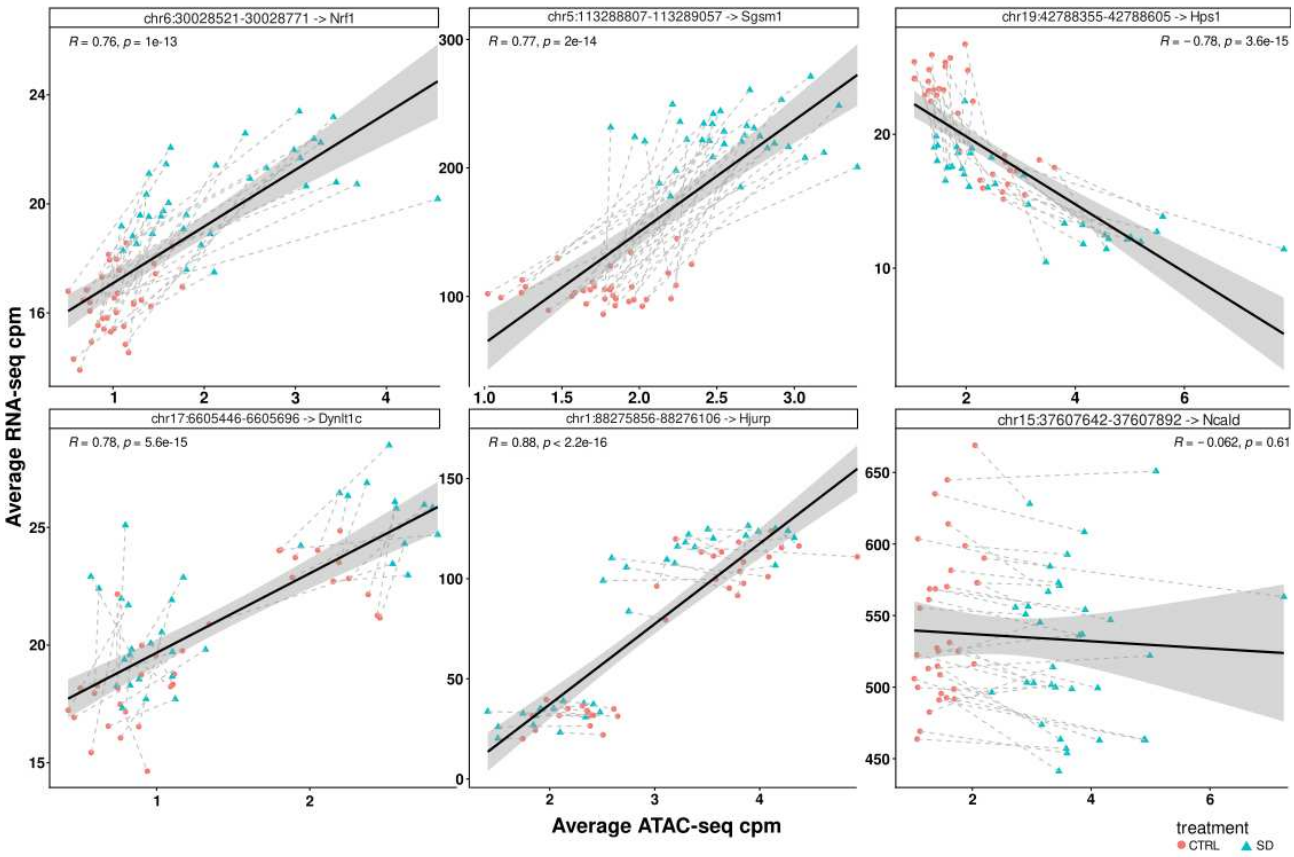


Figure S2:

Illustrative examples the of different types of accessibility/transcript correlations observed: negative correlation (*Hps1*), genetic/line-driven correlation (*Dynlt1c* and *Hjurp*), and treatment-driven correlation (*Nrf1* and *Sgsm1*) or both (*Hps1*). Lack of *Ncald* correlation with the most statistically significant region is also shown to highlight that highly statistical significant regions from ATAC-seq do not need to correlate with the annotated transcript. *Red*: Baseline counts per million (cpm); *blue*: cpm after SD.

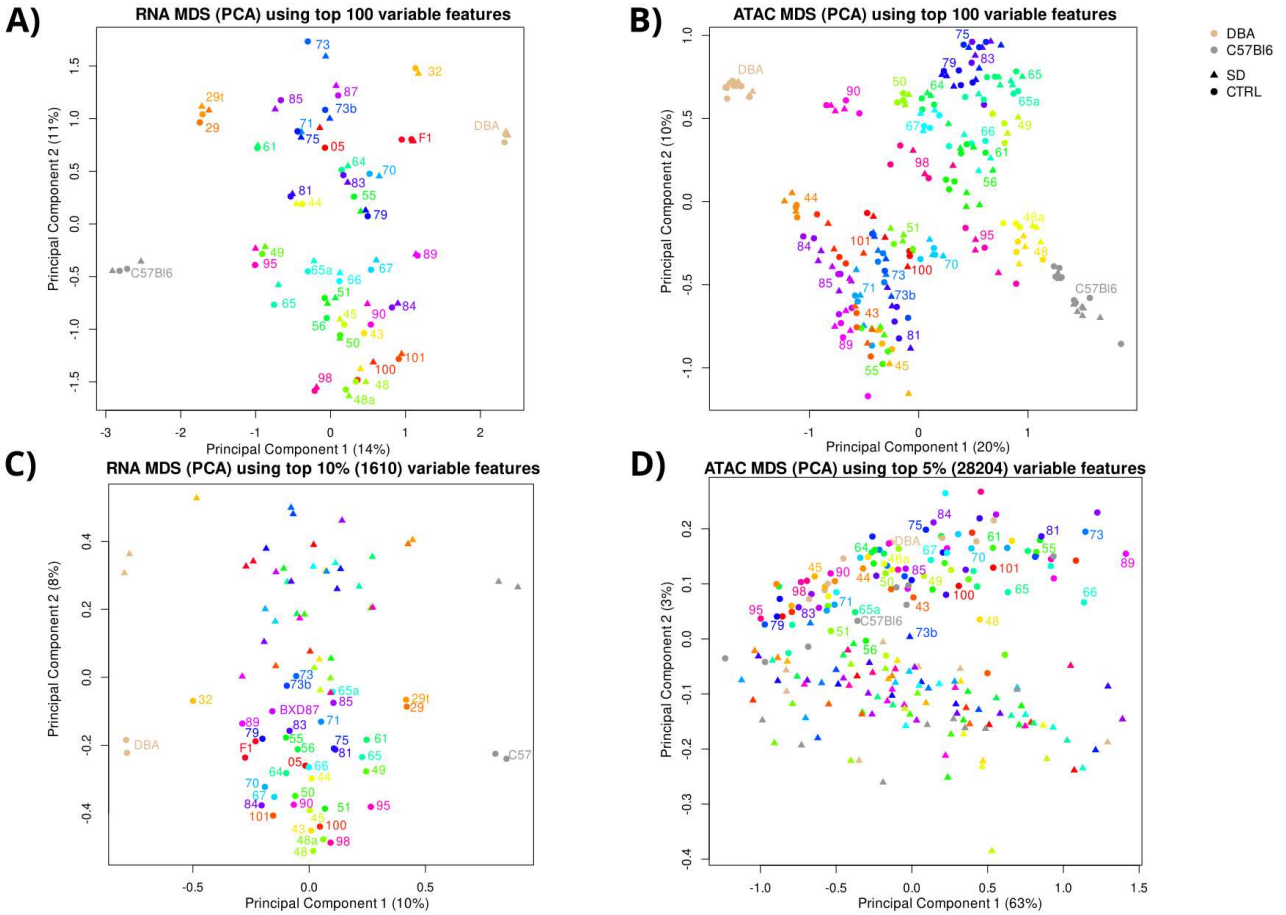


Figure S3:

Dimension reduction for the top 100 most variable features (transcripts/regions) for both **a)** transcriptome and **b)** chromatin accessibility, separates the samples mostly by BXD line but not SD. In particular, the parental lines are located at the extremes of principal component (PC) 1, indicating genetics have a higher impact on sample variability than SD. However, when considering additional features the effects of SD become noticeable among **c)** the top 10% most variable transcripts and **d)** top 5% of most variable accessibility, suggesting SD induces smaller, but more widespread changes.

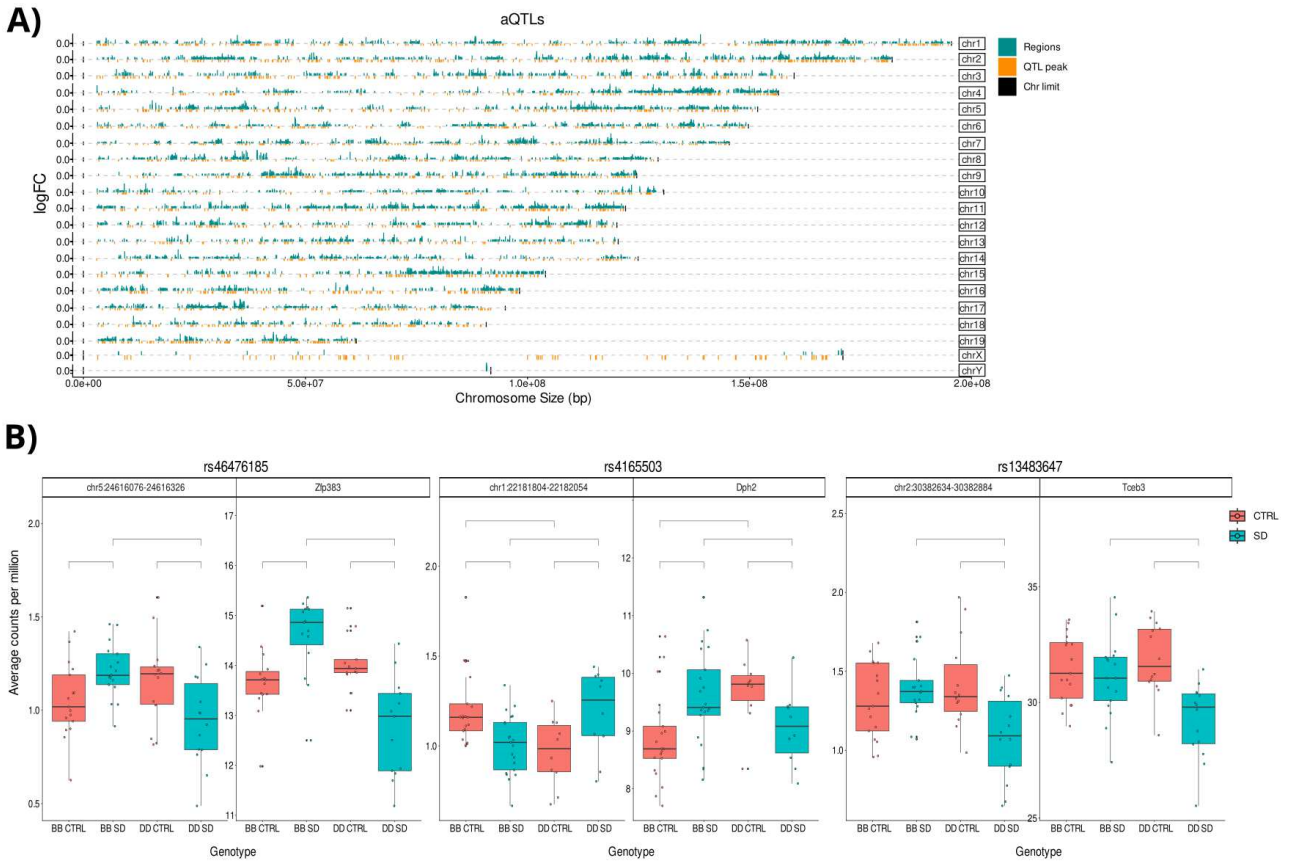


Figure S4:

a) Genomic distribution of all regions with significant aQTLs (green) and location of all LOD score peaks (orange). Chromosomes are displayed individually and their boundaries shown by black lines. **b)** Illustrative examples of genetic variants (SNPs) interacting with SD at both chromatin accessibility and transcript level: *rs46476185* is associated with no baseline differences (red CTRL) between B6-allele carriers (BB) and D2-allele carriers (DD) but opposed response to SD (increase in BB, decrease in DD); *rs4165503* is associated with different baseline levels and an opposed response to SD; *rs13483647* is associated with no baseline differences and with lack of SD response in BB- and a decrease in DD-carriers. *Red*: Baseline counts per million (cpm); *blue*: cpm after SD. Significant comparisons with *p*-value < 0.05 are indicated with bar on top connecting both groups tested.

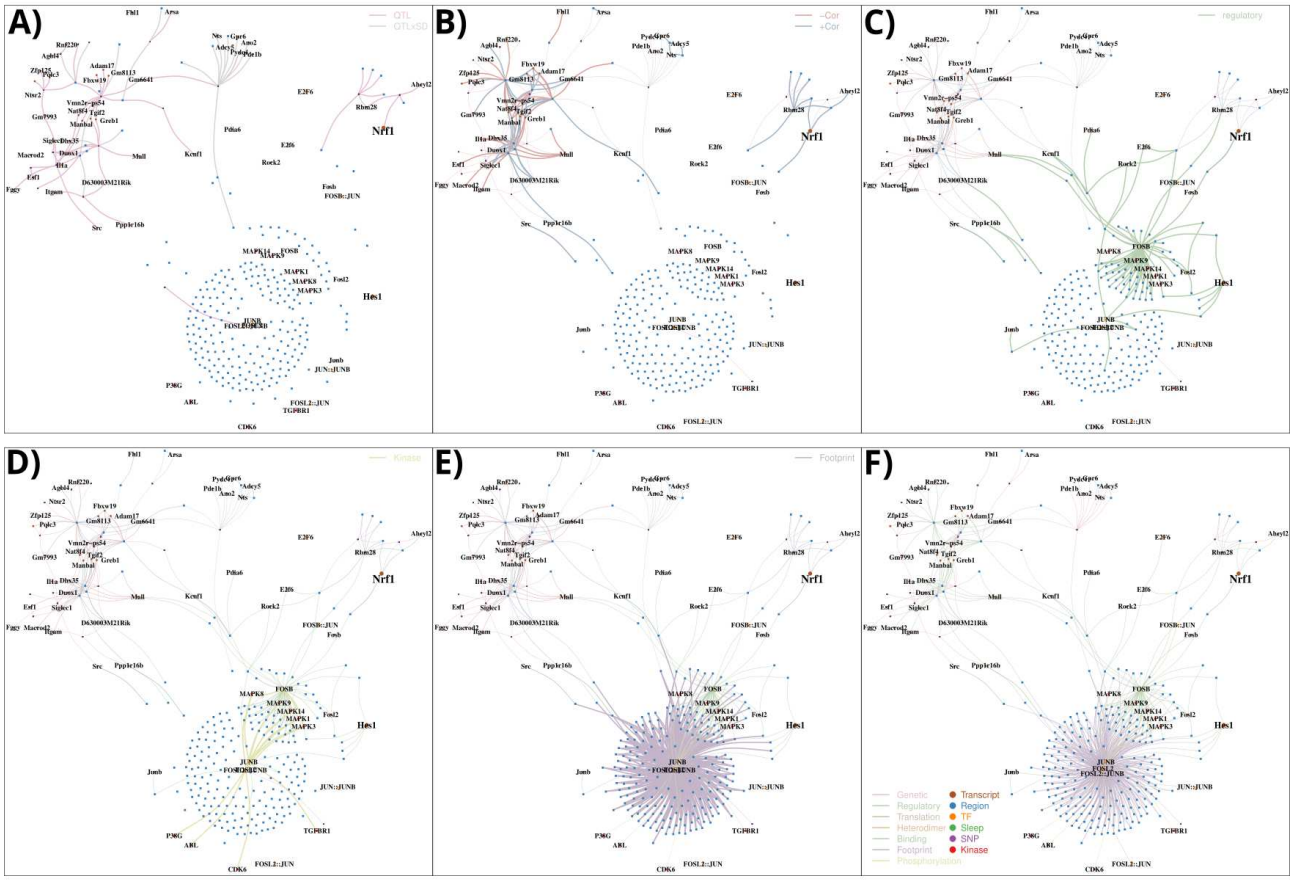


Figure S5:

Derivation of the SD-response network (SD-Net) illustrated by focusing on a subgraph of the network around *Nrf1* and *Hes1*. Chromatin regions (blue), transcripts (brown) and transcription factors (TFs - orange) were connected to genetic variants (SNPs - purple) by **a)** their baseline QTL LOD peak (pink) or their interaction QTLxSD LOD peak (gray). **b)** Regions and transcripts sharing an aQTL and eQTL LOD peak (SNP) were connected if their accessibility and transcripts level were significantly correlated (blue: positive correlation; red: negative correlation). This stage represents the system genetics sub-network (SG-sNet). **c)** The Gene Regulatory sub-Network (GR-sNet) was inferred using GraNIE (green) and added to the SG-sNet to form a unified genetic and gene regulatory network. **d)** The top enriched kinases (red) were connected to their TF targets (yellow). **e)** Chromatin regions were connected to all TF if these had at least one footprint identified within the region (purple). **f)** The resulting network (SD-Net) was pruned of footprint connections not matching other TF-region binding connections, regions with only one connection were removed, and only chromatin regions and transcripts significantly affected by SD were kept. The SD-Net edges were renamed to emphasize the biological meaning of the connection, instead of the analysis of origin. Thicker lines (edges) highlight the new connections added from the previous step.

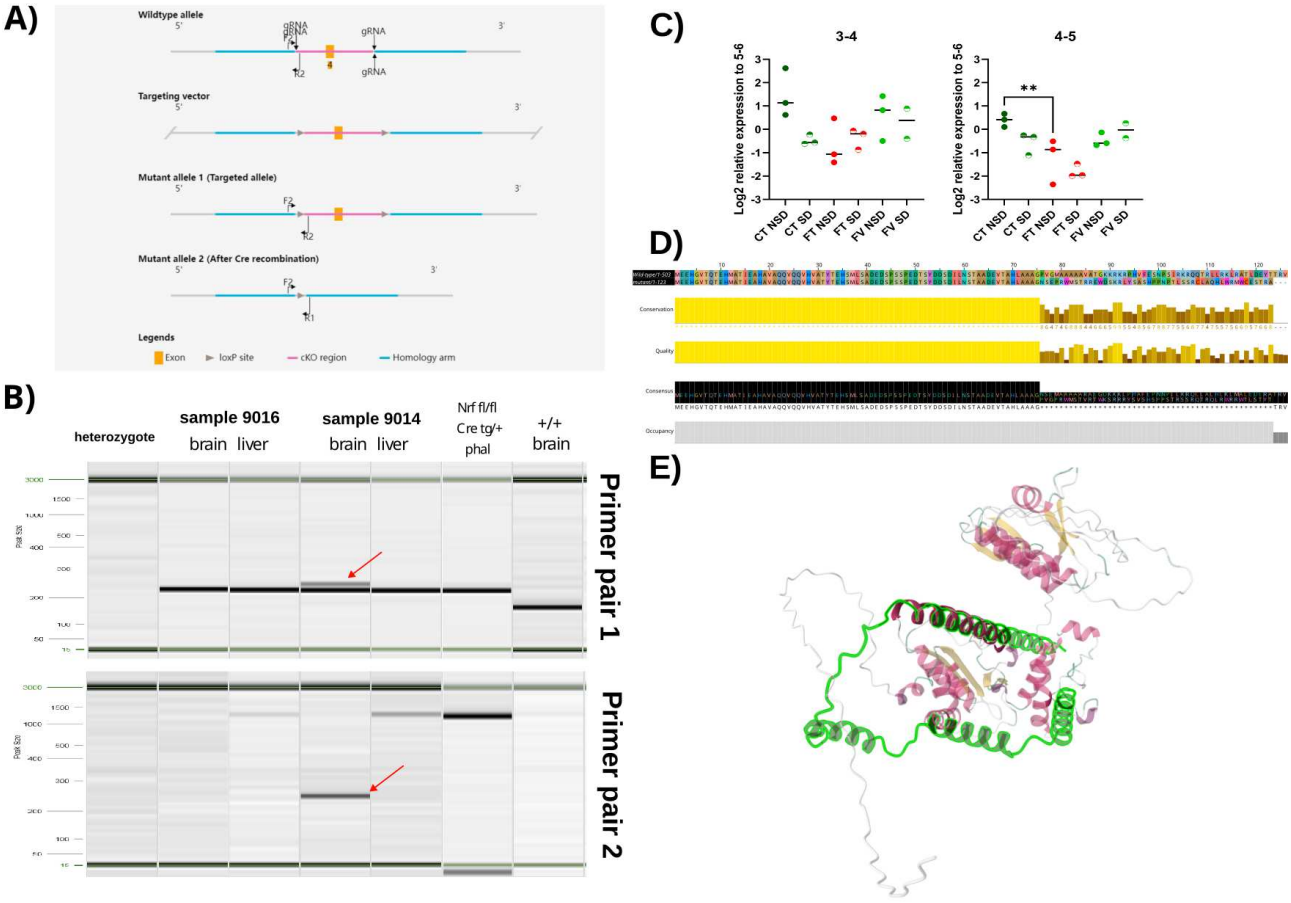


Figure S6:

a) Mutation strategy for insertion of LoxP sites flanking (flox) *Nrf1* exon 4. Conditional expression of CRE-ERT2 fusion driven by the *Camk2a* promoter (*Camk2a*-CreERT2), allows the specific recombination of the *floxed* region and removal of *Nrf1* exon 4 after treatment with tamoxifen. **b)** Validation of tamoxifen-induced conditional KO. Primer pair 1 was used as recommended by the supplier in a) to identify *Nrf1*$^{flox/flox}$ animals, illustrating changes in PCR product. However, given CRE activity is not ubiquitous, we further tested primer pair 2 which specifically amplifies exon 4. These primers produce an amplicon that is too large to be detectable unless exon 4 is excised from the genome, validating the tamoxifen effect. The amplicons of interest are highlighted with red arrows. Liver tissue was used as negative control for recombination. **c)** qPCR validation of the reduced use of the exon junctions 3-4 and 4-5 from the *Nrf1* transcript relative to exon junction 5-6 on the *Camk2a*-CreERT2$^{Tg/0}$/*Nrf1*$^{flox/flox}$ animals treated with tamoxifen compared to control animals. Since *Nrf1* is not mutated in every cell of the cortex, complete absence of these junctions is not expected, only differential exon usage. **d)** *In silico* translation of the expected *Nrf1* transcript sequence after removal of the exon 4. Removal of exon 4 leads to a 1bp frame-shift in the open reading frame, resulting in a premature stop codon and a truncated protein [70]. **e)** Comparison of the predicted NRF1 native conformation (alpha helices in pink, beta sheets in orange, unstructured regions in grey) and the truncated mutant protein expected to result (highlighted in green) from the excision of the exon 4. The initial alpha helix on the N-terminus side is predicted to be maintained for the mutant protein but the loss of the beta sheet leads to a mismatch in spatial conformation of the truncated protein.

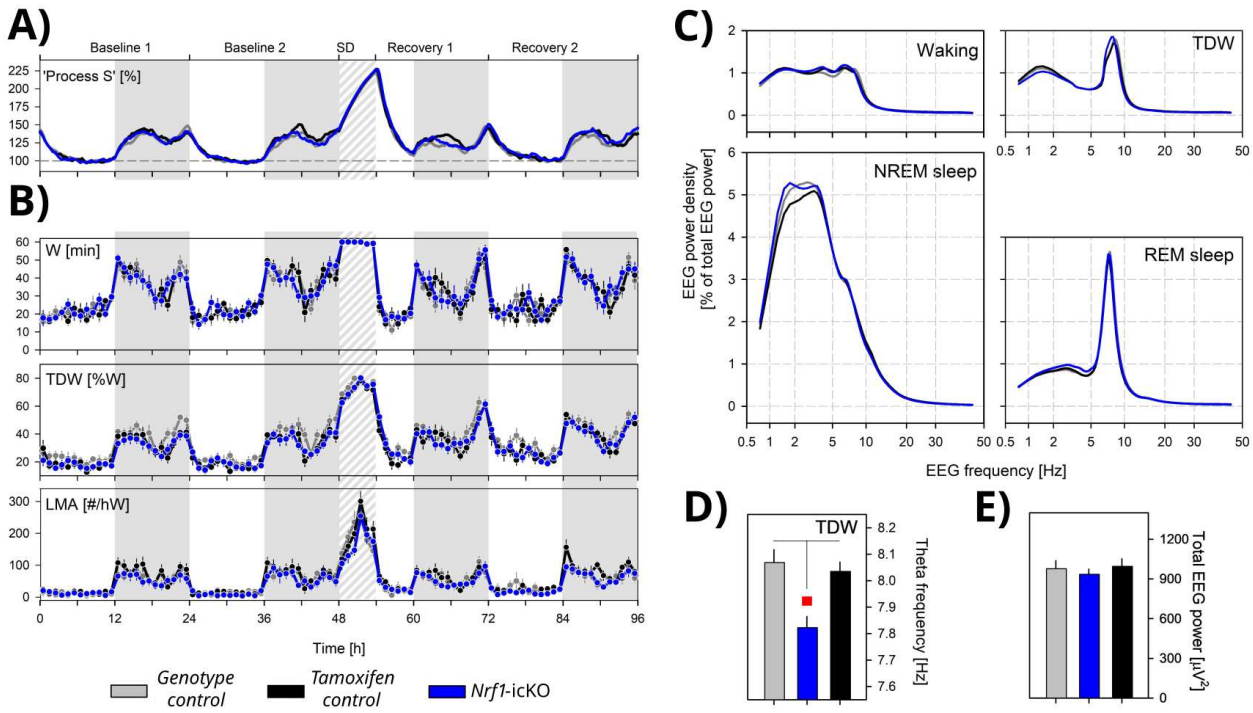


Figure S7:

a) Process S as predicted from the observed sleep-wake distribution shows no expected differences in the *Nrf1*-icKO animals. **b)** Time spent awake (minutes/h), in θ-dominated wake (TDW as % of time-spent-awake) and locomotor activity (LMA as counts per waking hour) over the course of the 4-day experiment, show no differences among experimental groups. **c)** No statistically significant differences in the spectral profiles for the different sleep-wake states were found. **d)** θ-peak frequency is slower in TDW for *Nrf1*-icKO animals compared to both control groups. **e)** No changes in total EEG power were detected between experimental groups (used as reference in c). All animals were kept of a 12/12h light dark cycle with lights on corresponding to ZT0 and light off to ZT12. *Baseline*: 0-48h; *SD*: 48-54h; *Recovery*: 54-96h. *gray*: *Camk2a*-CreERT2$^{Tg/0}$/*Nrf1*$^{+/+}$ animals treated with tamoxifen (Genotype control); *black*: *Camk2a-CreERT2*$^{Tg/0}$/*Nrf1*$^{flox/flox}$ animals treated with vehicle solution (Tamoxifen control); *blue*: *Camk2a*-CreERT2$^{Tg/0}$/*Nrf1*$^{flox/flox}$ animals treated with tamoxifen (induced and conditional knock-out - icKO).

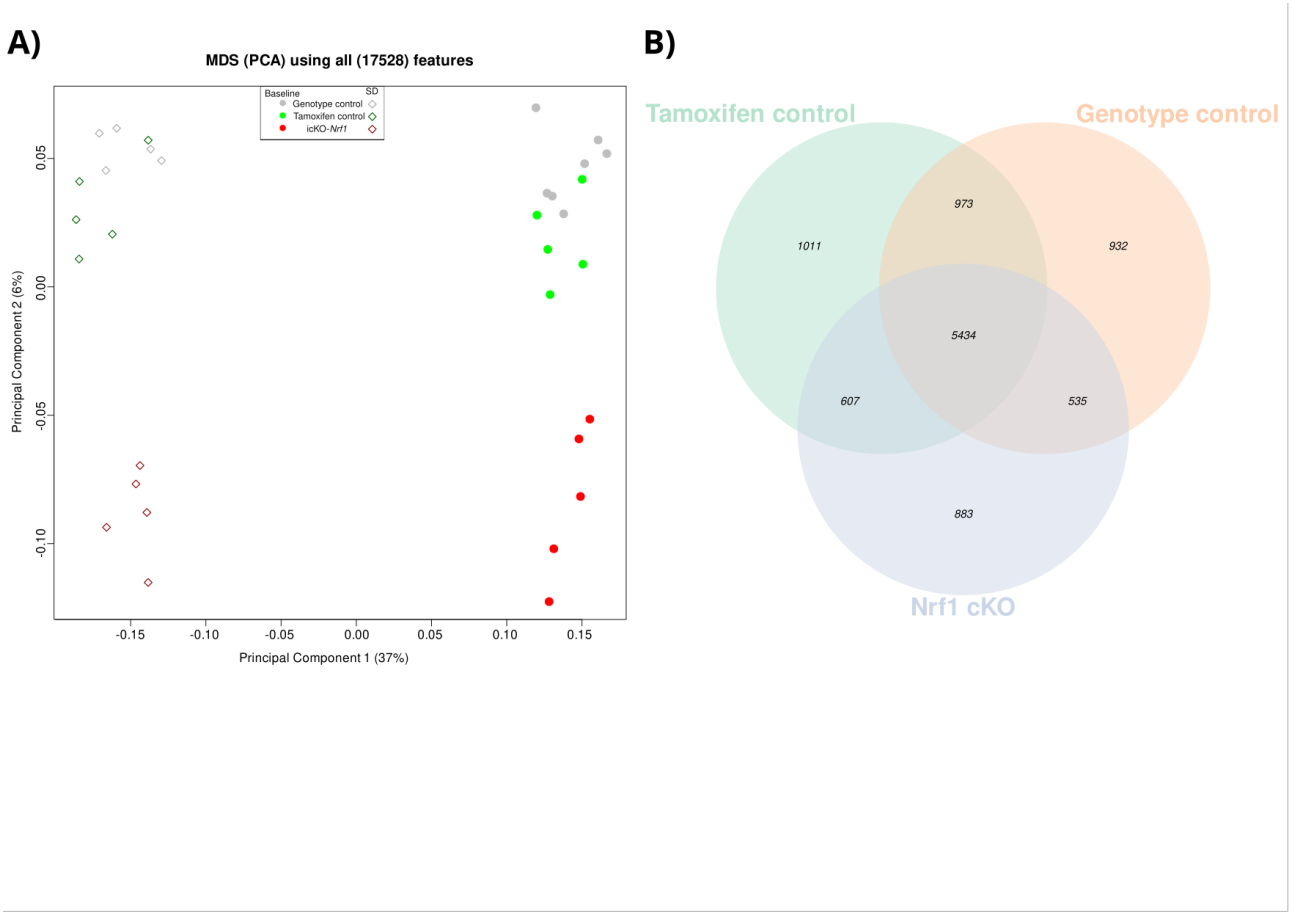


Figure S8:

a) Reduced dimensional projection of the transcriptomic data from *Nrf1*-icKO animals clearly shows a clustering between SD (Principal Component PC1) and icKO (PC2) samples from controls. **b)** Overlap of the SD effects on *Nrf1*-icKO compared to both genotype and tamoxifen control groups, highlights both specific and shared significant effects of SD among the three experimental groups.

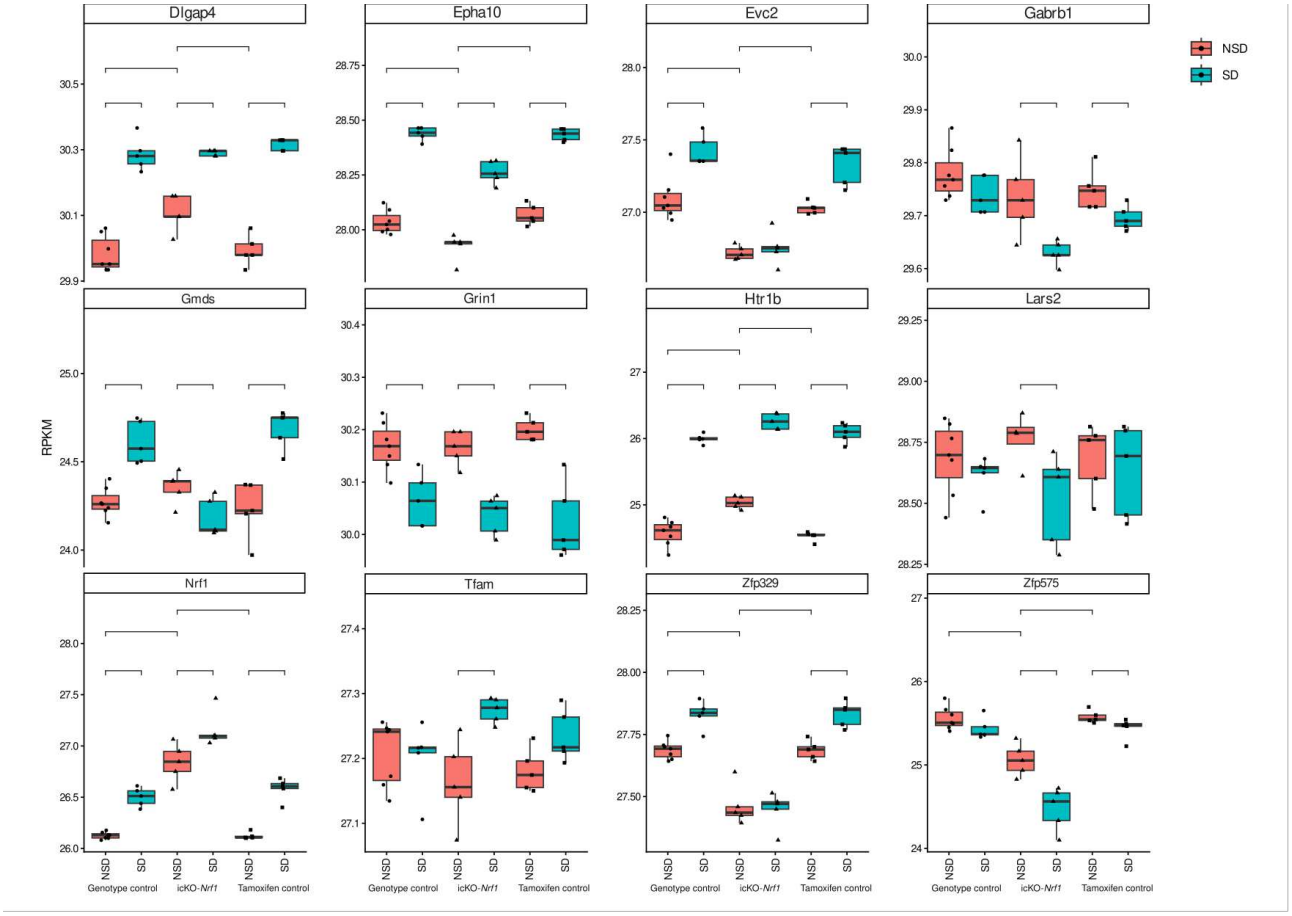


Figure S9:

Illustration of the transcription changes for some affected genes and previously described targets in the cortex of *Nrf1*-icKO mice. *RPKM*: reads per kilobase of gene per million reads. Significant comparisons with *p*-value < 0.05 are indicated with bar on top connecting both groups tested. *Red*: Non-sleep deprived (NSD) controls; *Blue*: Sleep deprived (SD) samples.

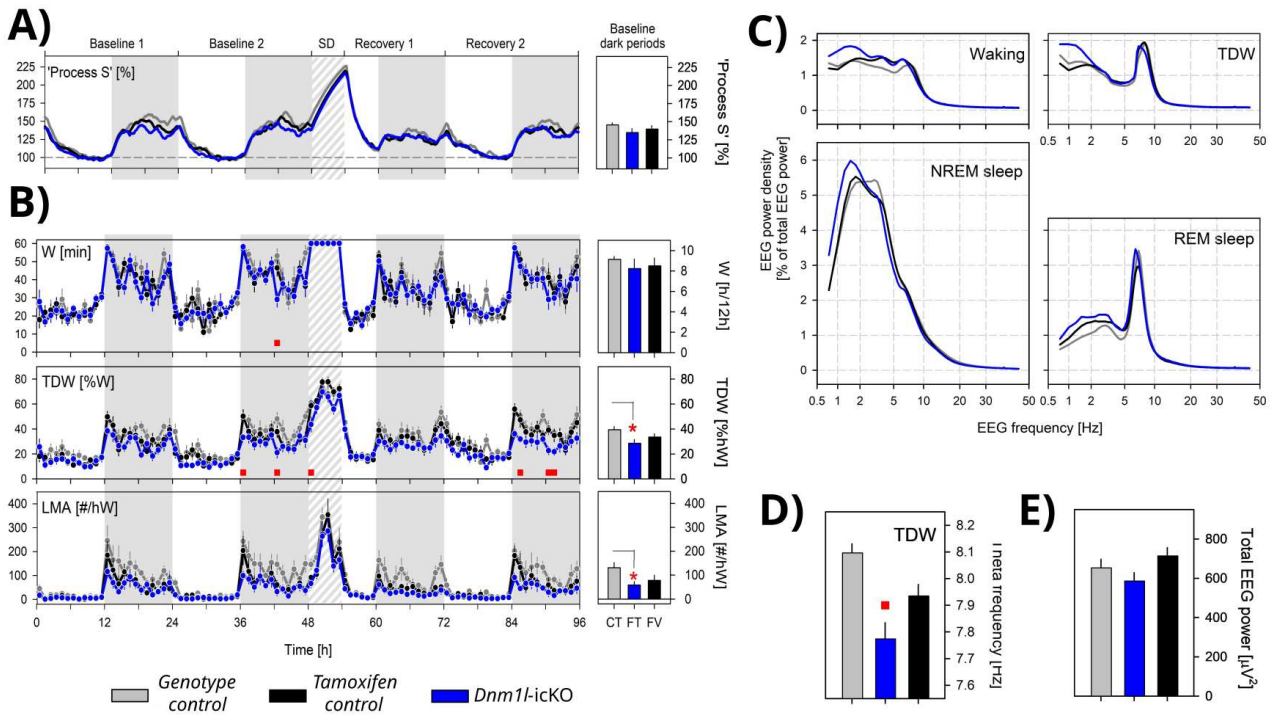


Figure S10:

a) Process S as predicted from the observed sleep-wake distribution shows no expected differences in the *Dnm1l*-icKO animals. **b)** Time spent awake (minutes/h), in θ-dominated wake (TDW as % of time-spent-awake) and locomotor activity (LMA as counts/ waking hour) over the course of the 4-day experiment. Quantification in the dark periods during the baseline show decreased TDW and locomotor activity in the *Dnm1l*-icKO animals. **c)** No statistically significant differences in the spectral profiles for the different sleep-wake states were found. **d)** θ-peak frequency is slower in TDW for *Dnm1l*-icKO animals compared to both control groups. **e)** No changes in total EEG power were detected between experimental groups (used as reference in c). All animals were kept of a 12/12h light dark cycle with lights on corresponding to ZT0 and light off to ZT12. Baseline: 0-48h; SD: 48-54h; Recovery: 54-96h. *gray*: *Camk2a*-CreERT2$^{Tg/0}$/*Dnm1l*$^{+/+}$ animals treated with tamoxifen (Genotype control); *black*: *Camk2a*-CreERT2$^{Tg/0}$/*Dnm1l*$^{flox/flox}$ animals treated with vehicle solution (Tamoxifen control); *blue*: *Camk2a*-CreERT2$^{Tg/0}$/*Dnm1l*$^{flox/flox}$ animals treated with tamoxifen (induced and conditional knock-out - icKO). Compare results to Figure S7.

Supplementary tables

Table S1: ATAC_QC_summary

Quality control (QC) summaries for the ATAC-seq data. *Sequencing*_QC shows the statistics for the sequencing quality as given by fastp [116] for each sample. *Aligment*_QC provides the alignment results from bowtie2 [117] for all samples. *Peak_QC* shows the peak calling statistics for each group of triplicates (BXD line/SD) by Genrich [120]. *Peak_Summary* summarizes the number of peaks identified for each group of triplicates, as well as how many base pairs and the percentage of genome are covered by these. *Merged_Peaks* lists the genomic coordinates for all 264'457 unique, non-overlapping identified peaks across all samples, and annotation to the nearest TSS. *Final_Peaks* shows the 775'292 genomic coordinates for the regions split into no longer than 250bp fragments, to avoid large regions and increase the resolution of the downstream analyses, as well as their annotation to the nearest TSS.

Table S2: Differential_Correlation

Results of differential and correlation statistical analyses for BXD lines. *Differential_Acessibility* shows genomic coordinates for all analyzed regions, the results for the differential accessibility analysis for the ATAC-seq data, the annotated transcript (nearest TSS) and the correlation (baseline, after SD and all samples) results between the region and transcript values. *Differential_Expression* summarizes the statistical result of the re-analysis of the RNA-seq data [16] for easier reference.

Table S3: Enrichment_BXD

Results of the gene set enrichment analysis (GSEA [40]) for the cortex ATAC-seq and RNA-seq on BXD population using Gene Ontology (*_GO*) and KEGG pathway (*_KEGG*) databases. O*verlap* shows the terms with exact match and shared genes between ATAC-seq and RNA-seq enrichment.

Table S4: Footprints

List of all footprints detected for each BXD line and treatment (if detected) by HINT-ATAC [46] listing the measured footprint score for each transcription factor (motif) binding to individual regions (chr, start, end). All regions are annotated to the closest transcriptional starting site for reference.

Table S5: KEA_enrichment

Kinase enrichment analisys (KEA3 [55]) integrated ranks from mean (*Mean_rank*) and top rank (*Integrated_scaled_rank*) metrics, connecting the transcription factors (TFs) predicted to have changed activity after SD to the kinases known to target them. Kinases in the top 50 results in both metrics are shown with * after their names.

Table S6: QTL

Quantitative trait locus (QTL) results for the cortex ATAC-seq, RNA-seq, estimated transcription factor activity *(TF)* and sleep phenotypes (pheno) on the BXD population, considering genetic associations on normalized counts corrected for SD (*_QTL*) or on average fold changes (*xSD_QTL*). *lod*: Logarithm of the odds; *chr*: QTL LOD peak chromossome; *pos*: location in centimorgan of the QTL LOD peak; *bp*: basepair (coordinate) estimation of the location of the QTL LOD peak; *_lo*: lower bound of the QTL 95% confidence interval; *_hi*: higher bound of the QTL 95% confidence interval; *_trend*: results for the screening for individual cases for baseline differences (BSL) or SD effects. *BB/DD*: number of BXD lines in each genotype. s*np*: Single nucleotide polymorphism matching the QTL peak. s*nps*: Single nucleotide polymorphism within the QTL confidence interval. *pheno_QTL* contains additional information on the sleep phenotypes [16], including labels used in figures. *Overlap_simple* shows the QTL overlaps between all analyses.

Table S7: GRN

Gene regulatory network (GR-sNet) inferred from ATAC-seq and RNA-seq data (GraNIE 58) including baseline and SD samples to enforce sleep-wake driven effects into the correlations. Statistics are shown for each TF-to-peak and peak-to-gene association. System Genetics Network (SG-sNet) inferred from the genetic associations found with the QTL analyses and chromatin accessibility/transcript correlations. Unfiltered Net represent the union of the previous two subnetworks. Final SD-Net edges and SD-net nodes for the final inferred network of the response to SD.

Table S8: RNA_QC_summary

Quality control (QC) summaries for the *Nrf1* conditional knock-out cortex RNA-seq data. *Sequencing*_QC shows the statistics for the sequencing quality as given by fastp [116] for each sample. *Aligment*_QC provides the alignment results from STAR [118] for all samples.

Table S9: Differential_expression

Results of differential for the *Nrf1* conditional knock-out cortex RNA-seq data. Two statistical models were considered: a simple SD vs Control on each separate animal group (*SD effect*); and an interaction model with conditional knock-out as reference comparison (-*Baseline*- and -*Interaction*-). *icKO*: *Nrf1* inducible and conditionally knock-out *Camk2a*-CreERT2$^{Tg/0}$/*Nrf1*$^{flox/flox}$ animals injected with tamoxifen. *Genotype control*: *Camk2a*-CreERT2$^{Tg/0}$/*Nrf1*$^{+/+}$ animals injected with tamoxifen. Tamoxifen *control*: *Camk2a*-CreERT2$^{Tg/0}$/*Nrf1*$^{flox/flox}$ animals injected with vehicle solution.

Methods

Animals

32 BXD/RwwJ advanced intercross (AI) recombinant inbred (RI) lines [20] in the Jackson Laboratory (https://www.jax.org/), including C57BL/6J and DBA/2J parental lines, were purchased from Charles River, France (www.criver.com). 8 shipments were made containing at least 1 pair of male animals of 10-12 weeks old per BXD line (matching CTRL and SD). One breeding pair of animals with LoxP sites inserted around *Nrf1* exon 4 were bought from Cyagen (https://www.cyagen.com/). B6;129S6-Tg(Camk2a-cre/ERT2)1Aibs/J (https://www.jax.org/strain/012362) kept at our animal facility were backcrossed to B6. Animals were kept in accordance with the Swiss Animal Protection Act, and all experimental procedures were approved by the veterinary authorities of the state of Vaud (Service de la Consommation et des Affaires Vétérinaires).

Nrf1 model validation

The *Ensembl* transcript and protein sequences for CCDS51741.1 were used as reference for the intron and exon annotation. The coding sequence from the wild-type reference and without exon 4 were then translated using the Expasy translation tool (https://www.expasy.org/). The identity of exon 4 was confirmed using the blat function of the UCSC genome browser (https://genome.ucsc.edu/index.html). Both sequences were aligned using Jalview (https://www.jalview.org/about/) to identify the effect of the excision of exon 4. Then AlphaFold Server (https://alphafoldserver.com/about) was used to model the protein structure. The two top structures were overlapped using RCSB PDB pairwise structure aliment tool (https://www.rcsb.org/alignment/).

To induce translocation to the nucleus of the fusion protein CRE-ERT2, allowing the recognition of LoxP sites by the CRE recombinase and genomic recombination of *Nrf1*, intraperitonial injections of 100 µL of tamoxifen (T5648-1g Sigma-Aldrich) were performed twice a day (around ZT0-1 and ZT6-7) for 5 consecutive days at a concentration of 10 mg/mL in sunflower seed oil (S5007-250ml Sigma-Aldrich) and 10% ethanol. Throughout the course of tamoxifen injections and one-week post-injection wait period, mice were closely monitored for any adverse reactions to the treatment. The mice were allowed to recover for 2 additional weeks before sleep recording.

The effect of tamoxifen injection on exon 4 excision was validated at the genomic level by end-point PCR (epPCR) on DNA extracted from cortex and liver (control tissue) using NaOH extraction method. Briefly, samples were incubated in 25 mM NaOH + 0.2 mM EDTA at 95ºC for 1 hour, 10% of solution volume of 40 mM Tris HCl pH 5.5 was added and the samples centrifuged 4000 rpm for 3 minutes to remove cellular debris. The primer pair recommended by Cyagen (forward: AAG ACT TGT ATG CAT TGG TCT CAG; reverse: TAG CAA ATT AAG GAA CTG GGT GAC) was used to to identify *Nrf1*$^{flox/flox}$ animals. Given that CRE-ERT2 is driven by the *Camk2a* promoter, not all cells in the cortex will be recombined, thus we designed an additional reverse primer using NCBI primer tool on NM_001164226.2 transcript (CCT GGG CTG CAG AAG TTT ACG TA), which would detect specifically the recombined amplicon when paired with the previous forward primer, as a second validation reaction.

The excision of the exon 4 was also confirmed at the transcript level. RNA was extracted from cortex samples using the Qiagen miRNAEasy micro kit (QIAGEN, 74004) with DNase digestion to remove

contaminating DNA. Complementary DNA (cDNA) was reverse synthesized using SuperScript II Reverse Transcriptase (Invitrogen, 18064014) using oligo(dT)15 (Promega, C110A) and random primers (Invitrogen, 48190011) and dNTP mix (Roche, 11581295001). The resulting cDNA was purified by digesting with Rnase H (New England Biolabs, M0297S). Usage of sequence spawning exon 3-4 (CTG CAG GTC CTG TGG GAA TG and AAG CAA ACG TGT CTG CTG TC), 4-5 (AGA AAC GGA AAC GGC CTC AT and GGC TCT GAG TTT CCG AAG CA) and 5-6 (CCT TTG GAG AAT GTG GTG CG and GAG GCG GCA GCT CTG AAT TA) were quantified for biological triplicates using quantitative PCR (qPCR). Both epPCR and qPCR were performed using miRCURY LNA SYBR Green PCR Kits (QIAGEN, 339345). Quantitative PCR was done using QuantStudio 6 Pro System (Applied Biosystems), using ROX reference at low concentration (200x dilution). Relative transcript quantification was estimated using the delta Ct method using the non-excised exons as reference (exon 5-6). After manually excluding results failing the melting curve and outlier analyses, the average Ct (amplification cycle detection threshold) obtained from three technical replicates was taken for each replicate/gene combination. The efficiency of the amplification was confirmed to not differ significantly from the theoretical value of 2 using serial dilution calibration method. The results were plotting using GraphPad Prism software. Primers were ordered from Lubio Science Switzerland (IDT distributor).

Sleep deprivation

10-12 weeks old male mice where were singly housed in our sleep-recording facility, with food and water available *ad libitum*, at a constant temperature of 25˚C and under a 12 h light/12 h dark cycle (LD12:12, fluorescent lights, intensity 6.6 cds/m^2, with ZT0 and ZT12 designating light and dark onset, respectively). Mice were allowed to acclimate to the sleep-recording facility for 2 to 4 weeks prior to the experiments. Animals were sleep-deprived (SD group) for 6 hours following the standard 'gentle handling' protocol [114], and a control group was allowed to sleep in parallel to establish the unperturbed baseline (CTRL group). Lines and treatment were randomized across the experimental cohorts so that biological replicates of 1 line were collected/recorded on more than 1 occasion while also ensuring that an even number of mice per line was included for tissue collection as to pair sleep deprived and baseline individuals within each cohort.

Animals used for sleep phenotyping were equipped with chronic EEG and EMG electrodes under deep anesthesia [114]. In short, intraperoneal injection of Xylazine (10 mg/kg)/Ketamine (100 mg/kg) was used to ensure deep anesthesia for the duration of the surgery (*i.e.*, around 30 min). Analgesia was provided the evening prior and the 3 days after surgery with Dafalgan in the drinking water (200–300 mg/kg). Mice were allowed to recover for at least 10 days prior to baseline recordings. EEG was recorded from 2 days (baseline, 48h) prior to SD until 2 days (42h) after SD, to monitor recovery. 11 *Camk2a*-CreERT2$^{Tg/0}$/*Nrf1*$^{flox/flox}$ were injected with tamoxifen (*Nrf1* icKO) and 11 with vehicle solution (tamoxifen control), and 10 *Camk2a*-CreERT2$^{Tg/0}$/*Nrf1*$^{+/+}$ were injected with tamoxifen (genotype control) for sleep phenotyping.

Animals used for molecular studies (ATAC- and RNA-sequencing) were killed and the end of the 6 hours SD together with circadian matching (ZT6) non-SD controls by decapitation after being anesthetized with isoflurane, upon which cerebral cortex was collected immediately. The cerebral cortex was rapidly dissected and flash-frozen in liquid nitrogen with the entire procedure taking no

longer than 5 minutes per animal. All samples were stored at −140°C until further use. At least 3 biological replicates for each BXD line and condition were used.

Sleep and spectral analyses

EEG and EMG signals were captured with a sampling rate of 2000Hz, amplified, filtered, digitized, and down-sampled and stored at 200Hz using EMBLA (Medcare Flaga, Thornton, CO, USA) hardware (A10 recorder) and software (Somnologica). LMA was recorded by passive infrared (PIR) sensors (Visonic, Tel Aviv, Israel) at 1 min resolution for the duration of the 4 day experiment, using ClockLab (ActiMetrics, IL, USA). Sleep-wake states were annotated visually by an expert according to established criteria [114], for consecutive 4s epochs, based on the EEG and EMG patterns. To determine spectral composition, EEG signals (0 to 90 Hz) underwent a discrete Fourier transformation, using a 4s windows (Hamming function), to determine power density at 0.25Hz resolution. Delta power (1-4Hz) was extracted for NREM sleep epochs, averaged over consecutive intervals to which an equal number of 4s NREM sleep epochs contributed (*i.e.* percentiles), and then expressed as a percentage of the levels reached between ZT8-12 (when both delta power and sleep homeostatic pressure reach lowest levels during baseline) during the 2 baseline days. SD and recovery time points were compared to baseline by means of 2-way repeated measures ANOVA followed by post-hoc Dunnett t-tests to compare each control to the induced conditional KO animals.

Sequencing and read counting

For the ATAC-seq, frozen cortical tissue was crushed and gently dissociated by pipetting in PBS-triton PI 2x 500µl followed by homogenization using a Dounce homogenizer with homogenizer pestle B in PBS, 10ml, 10% triton, 1 table of Complete nonEDTA (Merk,11873580001). 100’000 nuclei were used for the transposase reaction as previously described [34,115]. Size selection of the resulting DNA was perfumed using a 2% agarose gel, and the bands between 150 to 600bp were extracted using Qiaquick Gel extraction Kit (Qiagen; 28704). For RNA-seq, RNA was extracted from frozen cortical tissue extracted using miRNeasy Micro Kit (Qiagen, 217084). Libraries for ATAC-seq were prepared using Nextera XT DNA Library Preparation Kit (Illumina, FC-131-1024) and RNA-seq for *Nrf1*-icKO effects were prepared using the Illumina Stranded mRNA Prep (Ilumina, 20040532). Paired-end sequencing was performed by the Lausanne Genomic Technologies Facility (University of Lausanne, Switzerland), using a HiSeq 4000 SR System for ATAC-seq and Aviti SR for RNA-seq. All sequencing data is available on Gene Expression Omnibus *(*GEO ID: GSE303676).

Raw read length sequenced was 150bp. Sequenced read quality, trimming, and deduplication were performed with Fastp [116]. Base quality Phred score was above 30 (99.9% accuracy) for 94-96% (ATAC-seq) and 89-94% (RNA-seq) of the reads’ bases after filtering. Read duplication rates were between 6-55% (mean 22%; ATAC-seq) and 31-37% (mean 34%; RNA-seq). CG content was estimated to be between 42.2-47.4% (ATAC-seq) and 47.8-48.2% (RNA-seq), comparing to the overall mouse genomic CG content is estimated to be around 42% (**Table S1 and S9**). The reads were aligned to the mouse genome Dec 2011 (GRCm38/mm10) assembly reference using bowtie2 [117] (ATAC-seq) and STAR [118] (RNA-seq). MultiQC [119] was used to visualize read and alignment QC for all samples simultaneously. Unalignment rates were between 0.2-2.4% (ATAC-seq) and 1.9-4.5% (RNA-seq); with 47.4-67.1% (ATAC-seq) and 91.7-94.4% (RNA-seq) of unique mapping rates.

Peaks were called using Genrich [120] statistical processing, which is developed to handle duplicated samples, accounting for both black- and grey-listed regions (**Table S1**). The number of identified accessible genomic locations ranged from 9608 (BXD45-CTRL) to 208'075 (C57BL/6-SD). The fraction of reads in peaks (FRiP) was between 0.10-0.23. Having higher number of replicates, the parent strains C57BL/6J and DBA/2J contributed the most to the 264'457 unique non-overlapping regions were identified. These regions were further divided into 775'292 regions of sizes between 76 and 250bp to avoid statistical testing on extremely large regions and improve resolution. The genotype of the BXD animals was validated by variant calling on the available genomic reads using bcftools mpileup function and comparing to GeneNetwork (https://genenetwork.org/) reference genomes available in the R/qtl2 package [121]. Htseq [122] was used to count reads matching each of the identified regions for the ATAC-seq dataset.

Differential analyses

Both ATAC-seq and the RNA-seq read counts were analyzed for statistical differences using EdgeR package [102]. Effects of SD on chromatin accessibility were tested using BXD line as co-variate to account for the effects of genetics (~0 + BXD_line + SD) and testing for the SD coefficient with False Discovery Rate (FDR) < 0.05. Effects of SD in *Nrf1* icKO mice, having two controls, were analyzed either with a simple additive model (~Group); or including interaction effects (~Genotype x SD) considering the icKO (*Camk2a*-CreERT2$^{Tg/0}$/*Nrf1*$^{flox/flox}$ treated with tamoxifen) as the reference and testing for significant differences in both genotype control (*Camk2a*-CreERT2$^{Tg/0}$/*Nrf1*$^{+/+}$ treated with tamoxifen) or treatment control (*Camk2a*-CreERT2$^{Tg/0}$/*Nrf1*$^{flox/flox}$ treated with vehicle). Group was were defined as the combination of genotype and SD (*e.g.* icKO_SD), where genotype reflected the final genotype after tamoxifen/vehicle injection (icKO, *Nrf1*$^{flox/flox}$ or *Nrf1*$^{+/+}$).

QTL analysis

Quantitative trait locus (QTL) analyses were performed using the R/qtl2 package [121], excluding the parent lines from the analysis to remove potential biases due to the lack of variability and larger number of replicate samples. Pseudo-markers were inserted at 1cM intervals to estimate a kinship matrix for the BXD lines using the leave one chromosome out method [123]. The additive model was obtained by scanning for associations using SD as a co-variate, while the interaction model was obtained using the log2 average fold change in response to SD. Sexual chromosomes were scanned independently from autosomes and statistical significance was obtained using a logarithm of the odds (LOD) cut-off estimated using 200 permutations. The base pair position for the QTL regions was estimated by converting the location of the annotated SNP/variants from cM to base pair (bp) using the mm10 mouse reference genome. QTLs with an imbalance of allelic distribution of a variant (B6 or D2), defined as one allele being present in less than 5 BXD lines, were excluded from the final QTL results.

We screened the significant results to identify the underlying effects of the genetic variant on the response to SD. For each QTL identified, the samples were split by genotype (B6 or D2) of the SNP at the peak LOD score and t-tests were performed on the normalized counts to identify differences in the baseline and SD effects on both genotypes. QTLs where the SD effect was significant for one genotype but not the other were classified as "Protected SD effect". If both were significant but had

opposite changes, these were classified as “Opposite SD effect”. Likewise, if both genotypes responded significantly in the same direction they were classified as either “Up” or “Down”. In addition, the QTLs were also screened for differences in the baseline.

To ensure methodological consistency, we replicated the previous QTL analysis for the previously measured phenotypes and transcriptome [16], and additionally for the newly predicted TF activities obtained from our footprint analysis (**Table S6**).

Footprint analysis

Footprints were identified for the regions showing statistically significant changes in accessibility after SD using HINT-ATAC [46]. The identified footprints were matched to the binding motifs in the JASPAR database [124]. Since HINT-ATAC [46] does not provide a statistical test for more than one comparison (across BXD lines), the transcriptional activity changes were estimated for each line separately. The results were then aggregated using the Fisher's combined probability test and average activity changes were reported (**Figure 2b**). However, comparison using all samples was used to obtain normalized activity scored in order all to visualize samples simultaneously (**Figure 2a**).

Functional annotations

Genomic regions which were annotated to their closest annotated Transcription Starting Site (TSS) and any overlapping candidate *cis* regulatory element from ENCODE’s Registry of cCREs database (https://screen.wenglab.org/about) using the ChipSeeker [125] and annotatr [126] packages. Enrichment analysis was done with the Clusterprofiler [127] implementation of Gene Set Enrichment analysis (GSEA) [40] using the Gene Ontology (GO [128]) and Kyoto Encyclopedia of Genes and Genomes (KEGG [129]) knowledge bases. Accessibility estimates for all regions annotating one gene were averaged and sorted by average log2 fold-change. Gene missing ENTREZID or not detected in the previous transcriptomic study [16] were excluded from the analysis. Kinase enrichment analysis was performed using KEA3 [55] with all the TFs identified with the footprint analysis as significantly affected across the BXD lines as input.

Network analyses

The systems genetics network (SG-sNet) was inferred using the QTL analyses results (Table S6). Genetic variants (SNPs) were considered the source node and connected by QTLs or interaction QTLxSDs to their target nodes (transcripts, chromatin regions, TFs, or sleep phenotypes). Pearson correlations were estimated for chromatin regions and transcripts sharing a edge to a SNPs and an edge was established between the two if the correlation was significant (p-value < 0.05). The gene-regulatory network (GR-sNet) was inferred using the GraNIE package 58 with unfiltered counts for the RNA-seq and ATAC-seq data, to establish unbiased region-to-transcript and TF-to-region connections. These two networks were connected using the igraph R package. The top enriched kinases identified in our KEA3 55 analysis were connected to their target TFs and footprints identified in any BXD strain were added between TFs and chromatin regions. In order to simplify the complex web of interactions, we filtered the network for transcript and chromatin regions significantly affected by SD, kept only footprint edges for regions with other connections to TFs, and pruned any peripheral nodes (e.g. chromatin regions and TFs associated with only 1 other entity), and then we connected any

TF to its transcript or heterodimer, if present in the network. The qgraph R package implementation of the Fruchterman-Reingold-Algorithm was used to obtain the force-directed graph layout used for plotting the networks.

Declaration of interests

The authors declare no competing interests.

References

1. Benington, J. H. & Heller, H. C. Restoration of brain energy metabolism as the function of sleep. *Progress in Neurobiology* **45**, 347–360 (1995).
2. Krueger, J. M. *et al.* Sleep as a fundamental property of neuronal assemblies. *Nature Reviews Neuroscience* **9**, 910–919 (2008).
3. Tononi, G. & Cirelli, C. Sleep and the price of plasticity: from synaptic and cellular homeostasis to memory consolidation and integration. *Neuron* **81**, 12–34 (2014).
4. Xie, L. *et al.* Sleep Drives Metabolite Clearance from the Adult Brain. *Science* **342**, 373–377 (2013).
5. Franken, P. & Dijk, D.-J. Sleep and circadian rhythmicity as entangled processes serving homeostasis. *Nat Rev Neurosci* **25**, 43–59 (2024).
6. Hagewoud, R. *et al.* Sleep deprivation impairs spatial working memory and reduces hippocampal AMPA receptor phosphorylation. *Journal of Sleep Research* **19**, 280–288 (2010).
7. Xu, Z.-Q., Gao, C.-Y., Fang, C.-Q., Zhou, H.-D. & Jiang, X.-J. The Mechanism and Characterization of Learning and Memory Impairment in Sleep-Deprived Mice. *Cell Biochemistry and Biophysics* **58**, 137–140 (2010).
8. Nwaogu, J. M., Chan, A. P. C., Naslund, J. A. & Anwer, S. The Interplay Between Sleep and Safety Outcomes in the Workplace: A Scoping Review and Bibliographic Analysis of the Literature. *International Journal of Environmental Research and Public Health* **22**, (2025).
9. Beihl, D. A., Liese, A. D. & Haffner, S. M. Sleep Duration as a Risk Factor for Incident Type 2 Diabetes in a Multiethnic Cohort. *Annals of Epidemiology* **19**, 351–357 (2009).
10. Cappuccio, F. P. *et al.* Meta-Analysis of Short Sleep Duration and Obesity in Children and Adults. *Sleep* **31**, 619–626 (2008).
11. Chaput, J.-P., Després, J.-P., Bouchard, C. & Tremblay, A. The Association Between Sleep Duration and Weight Gain in Adults: A 6-Year Prospective Study from the Quebec Family Study. *Sleep* **31**, 517–523 (2008).
12. Grandner, M. A., JACKSON, N. J., PAK, V. M. & GEHRMAN, P. R. Sleep disturbance is associated with cardiovascular and metabolic disorders. *Journal of Sleep Research* **21**, 427–433 (2012).
13. Kim, C.-W., Chang, Y., Kang, J.-G. & Ryu, S. Changes in sleep duration and subsequent risk of hypertension in healthy adults. *Sleep* **41**, zsy159 (2018).
14. Shi, L. *et al.* Sleep disturbances increase the risk of dementia: A systematic review and meta-analysis. *Sleep Medicine Reviews* **40**, 4–16 (2018).
15. Andretic, R., Franken, P. & Tafti, M. Genetics of sleep. *Annu Rev Genet* **42**, 361–388 (2008).
16. Diessler, S. *et al.* A systems genetics resource and analysis of sleep regulation in the mouse. *PLoS Biol* **16**, e2005750 (2018).

17. Funato, H. *et al.* Forward-genetics analysis of sleep in randomly mutagenized mice. *Nature* **539**, 378–383 (2016).
18. Koh, K. *et al.* Identification of SLEEPLESS, a Sleep-Promoting Factor. *Science* **321**, 372–376 (2008).
19. Mang, G. M. & Franken, P. Genetic dissection of sleep homeostasis. *Curr Top Behav Neurosci* **25**, 25–63 (2015).
20. Peirce, J. L., Lu, L., Gu, J., Silver, L. M. & Williams, R. W. A new set of BXD recombinant inbred lines from advanced intercross populations in mice. *BMC Genetics* **5**, 7 (2004).
21. Cirelli, C., Gutierrez, C. M. & Tononi, G. Extensive and Divergent Effects of Sleep and Wakefulness on Brain Gene Expression. *Neuron* **41**, 35–43 (2004).
22. Muheim, C. M. *et al.* Ontogenesis of the molecular response to sleep loss. *Neurobiology of Sleep and Circadian Rhythms* **14**, 100092 (2023).
23. Noya, S. B. *et al.* The forebrain synaptic transcriptome is organized by clocks but its proteome is driven by sleep. *Science* **366**, eaav2642 (2019).
24. Vanrobaeys, Y. *et al.* Mapping the spatial transcriptomic signature of the hippocampus during memory consolidation. *Nature Communications* **14**, 6100 (2023).
25. Brüning, F. *et al.* Sleep-wake cycles drive daily dynamics of synaptic phosphorylation. *Science* **366**, eaav3617 (2019).
26. Ode, K. L. & Ueda, H. R. Phosphorylation Hypothesis of Sleep. *Frontiers in Psychology* **Volume 11-2020**, (2020).
27. Wang, Z. *et al.* Quantitative phosphoproteomic analysis of the molecular substrates of sleep need. *Nature* **558**, 435–439 (2018).
28. Alfonsa, H. *et al.* Intracellular chloride regulation mediates local sleep pressure in the cortex. *Nature Neuroscience* **26**, 64–78 (2023).
29. Dietz, A. G. *et al.* Local extracellular K^+ in cortex regulates norepinephrine levels, network state, and behavioral output. *Proceedings of the National Academy of Sciences* **120**, e2305071120 (2023).
30. Forsberg, M. *et al.* Ion concentrations in cerebrospinal fluid in wakefulness, sleep and sleep deprivation in healthy humans. *Journal of Sleep Research* **31**, e13522 (2022).
31. Krone, L. B. *et al.* A role for the cortex in sleep-wake regulation. *Nat Neurosci* **24**, 1210–1215 (2021).
32. Vaidyanathan, T. V., Collard, M., Yokoyama, S., Reitman, M. E. & Poskanzer, K. E. Cortical astrocytes independently regulate sleep depth and duration via separate GPCR pathways. *Elife* **10**, (2021).
33. Chen, Y. *et al.* Chromatin accessibility: biological functions, molecular mechanisms and therapeutic application. *Signal Transduction and Targeted Therapy* **9**, 340 (2024).
34. Hor, C. N. *et al.* Sleep–wake-driven and circadian contributions to daily rhythms in gene expression and chromatin accessibility in the murine cortex. *Proceedings of the National Academy of Sciences* **116**, 25773–25783 (2019).
35. Haynes, P. R. *et al.* A neuron–glia lipid metabolic cycle couples daily sleep to mitochondrial homeostasis. *Nature Neuroscience* **27**, 666–678 (2024).
36. Sarnataro, R., Velasco, C. D., Monaco, N., Kempf, A. & Miesenböck, G. Mitochondrial origins of the pressure to sleep. *Nature* **645**, 722–728 (2025).
37. Abascal, F. *et al.* Expanded encyclopaedias of DNA elements in the human and mouse genomes. *Nature* **583**, 699–710 (2020).

38. Phillips, J. E. & Corces, V. G. CTCF: master weaver of the genome. *Cell* **137**, 1194–1211 (2009).
39. Chen, K.-F., Lowe, S., Lamaze, A., Krätschmer, P. & Jepson, J. Neurocalcin regulates nighttime sleep and arousal in *Drosophila*. *eLife* **8**, e38114 (2019).
40. Subramanian, A. *et al.* Gene set enrichment analysis: A knowledge-based approach for interpreting genome-wide expression profiles. *Proceedings of the National Academy of Sciences* **102**, 15545–15550 (2005).
41. Maret, S. *et al.* Homer1a is a core brain molecular correlate of sleep loss. *Proc Natl Acad Sci U S A* **104**, 20090–20095 (2007).
42. Sullivan, K. R., Ravens, A., Walker, A. C. & Shepherd, J. D. "Arc – A viral vector of memory and synaptic plasticity". *Current Opinion in Neurobiology* **91**, 102979 (2025).
43. Sun, X. & Lin, Y. Npas4: Linking Neuronal Activity to Memory. *Trends Neurosci* **39**, 264–275 (2016).
44. Yang, W. *et al.* Rheb mediates neuronal-activity-induced mitochondrial energetics through mTORC1-independent PDH activation. *Dev Cell* **56**, 811-825.e6 (2021).
45. Zhou, J. *et al.* NMDA receptor-dependent prostaglandin-endoperoxide synthase 2 induction in neurons promotes glial proliferation during brain development and injury. *Cell Rep* **38**, 110557 (2022).
46. Li, Z. *et al.* Identification of transcription factor binding sites using ATAC-seq. *Genome Biology* **20**, 45 (2019).
47. Pellegrino, R. *et al.* A novel BHLHE41 variant is associated with short sleep and resistance to sleep deprivation in humans. *Sleep* **37**, 1327–1336 (2014).
48. Bunger, M. K. *et al.* Mop3 is an essential component of the master circadian pacemaker in mammals. *Cell* **103**, 1009–1017 (2000).
49. Neves, C., Hor, C. N., Jimenez, S. & Franken, P. The sleep-wake history contributes to rhythmic BMAL1 chromatin binding in the cerebral cortex but not in the liver. *Proc Natl Acad Sci U S A* **122**, e2515047122 (2025).
50. Matsuzaki, T., Yoshihara, T., Ohtsuka, T. & Kageyama, R. Hes1 expression in mature neurons in the adult mouse brain is required for normal behaviors. *Scientific Reports* **9**, 8251 (2019).
51. Jeyaraj, D. *et al.* Klf15 Orchestrates Circadian Nitrogen Homeostasis. *Cell Metabolism* **15**, 311–323 (2012).
52. Güntan, İ. *et al.* Diurnal dynamics of the Zbtb14 protein in the ventral hippocampus are disrupted in epileptic mice. *Neuroscience* **569**, 12–20 (2025).
53. Wapinski, O. L. *et al.* Hierarchical Mechanisms for Direct Reprogramming of Fibroblasts to Neurons. *Cell* **155**, 621–635 (2013).
54. Massaro, M., Baudo, G., Lee, H., Liu, H. & Blanco, E. Nuclear respiratory factor-1 (NRF1) induction drives mitochondrial biogenesis and attenuates amyloid beta-induced mitochondrial dysfunction and neurotoxicity. *Neurotherapeutics* **22**, e00513 (2025).
55. Kuleshov, M. V. *et al.* KEA3: improved kinase enrichment analysis via data integration. *Nucleic Acids Res* **49**, W304–W316 (2021).
56. Mulligan, M. K., Mozhui, K., Prins, P. & Williams, R. W. GeneNetwork: A Toolbox for Systems Genetics. *Methods Mol Biol* **1488**, 75–120 (2017).
57. Jan, M., O'Hara, B. F. & Franken, P. Recent advances in understanding the genetics of sleep. *F1000Res* **9**, F1000 Faculty Rev-214 (2020).

58. Kamal, A. *et al.* GRaNIE and GRaNPA: inference and evaluation of enhancer‐mediated gene regulatory networks. *Molecular Systems Biology* **19**, e11627 (2023).
59. Ng, M. & Pavlova, M. Why are seizures rare in rapid eye movement sleep? Review of the frequency of seizures in different sleep stages. *Epilepsy Res Treat* **2013**, 932790 (2013).
60. Seugnet, L. *et al.* Notch signaling modulates sleep homeostasis and learning after sleep deprivation in Drosophila. *Curr Biol* **21**, 835–840 (2011).
61. Larsson, N.-G. *et al.* Mitochondrial transcription factor A is necessary for mtDNA maintance and embryogenesis in mice. *Nature Genetics* **18**, 231–236 (1998).
62. Zhang, W., Liu, D., Yuan, M. & Zhu, L.-Q. The mechanisms of mitochondrial abnormalities that contribute to sleep disorders and related neurodegenerative diseases. *Ageing Research Reviews* **97**, 102307 (2024).
63. Hartmann, C. & Kempf, A. Mitochondrial control of sleep. *Curr Opin Neurobiol* **81**, 102733 (2023).
64. Reimund, E. The free radical flux theory of sleep. *Medical Hypotheses* **43**, 231–233 (1994).
65. Chang, W.-T., Chen, H., Chiou, R.-J., Chen, C.-Y. & Huang, A.-M. A novel function of transcription factor α-Pal/NRF-1: Increasing neurite outgrowth. *Biochemical and Biophysical Research Communications* **334**, 199–206 (2005).
66. Dhar, S. S., Liang, H. L. & Wong-Riley, M. T. T. Nuclear respiratory factor 1 co-regulates AMPA glutamate receptor subunit 2 and cytochrome c oxidase: tight coupling of glutamatergic transmission and energy metabolism in neurons. *J Neurochem* **108**, 1595–1606 (2009).
67. Dhar, S. S. & Wong-Riley, M. T. T. Coupling of energy metabolism and synaptic transmission at the transcriptional level: role of nuclear respiratory factor 1 in regulating both cytochrome c oxidase and NMDA glutamate receptor subunit genes. *J Neurosci* **29**, 483–492 (2009).
68. Li, Z., Cogswell, M., Hixson, K., Brooks-Kayal, A. R. & Russek, S. J. Nuclear Respiratory Factor 1 (NRF-1) Controls the Activity Dependent Transcription of the GABA-A Receptor Beta 1 Subunit Gene in Neurons. *Front Mol Neurosci* **11**, 285 (2018).
69. Huo, L. & Scarpulla, R. C. Mitochondrial DNA instability and peri-implantation lethality associated with targeted disruption of nuclear respiratory factor 1 in mice. *Mol Cell Biol* **21**, 644–654 (2001).
70. Kiyama, T. *et al.* Essential roles of mitochondrial biogenesis regulator Nrf1 in retinal development and homeostasis. *Molecular Neurodegeneration* **13**, 56 (2018).
71. Tatsuki, F. *et al.* Involvement of Ca2+-Dependent Hyperpolarization in Sleep Duration in Mammals. *Neuron* **90**, 70–85 (2016).
72. Wang, X., Zhang, C., Szábo, G. & Sun, Q.-Q. Distribution of CaMKIIα expression in the brain in vivo, studied by CaMKIIα-GFP mice. *Brain Res* **1518**, 9–25 (2013).
73. Franken, P., Chollet, D. & Tafti, M. The Homeostatic Regulation of Sleep Need Is under Genetic Control. *Journal of Neuroscience* **21**, 2610–2621 (2001).
74. Vassalli, A. & Franken, P. Hypocretin (orexin) is critical in sustaining theta/gamma-rich waking behaviors that drive sleep need. *Proceedings of the National Academy of Sciences* **114**, E5464–E5473 (2017).
75. Borbély, A. A., Daan, S., Wirz-Justice, A. & Deboer, T. The two-process model of sleep regulation: a reappraisal. *J Sleep Res* **25**, 131–143 (2016).
76. Hubbard, J. *et al.* Rapid fast-delta decay following prolonged wakefulness marks a phase of wake-inertia in NREM sleep. *Nat Commun* **11**, 3130 (2020).

77. Boutrel, B., Franc, B., Hen, R., Hamon, M. & Adrien, J. Key role of 5-HT1B receptors in the regulation of paradoxical sleep as evidenced in 5-HT1B knock-out mice. *J Neurosci* **19**, 3204–3212 (1999).
78. Oettinghaus, B. *et al.* Synaptic dysfunction, memory deficits and hippocampal atrophy due to ablation of mitochondrial fission in adult forebrain neurons. *Cell Death & Differentiation* **23**, 18–28 (2016).
79. Kempf, A., Song, S. M., Talbot, C. B. & Miesenböck, G. A potassium channel β-subunit couples mitochondrial electron transport to sleep. *Nature* **568**, 230–234 (2019).
80. Andrews, S. J., Das, D., Anstey, K. J. & Easteal, S. Association of AKAP6 and MIR2113 with cognitive performance in a population-based sample of older adults. *Genes Brain Behav* **16**, 472–478 (2017).
81. Bramham, C. R., Worley, P. F., Moore, M. J. & Guzowski, J. F. The immediate early gene arc/arg3.1: regulation, mechanisms, and function. *J Neurosci* **28**, 11760–11767 (2008).
82. Kim, D. W., Moon, H. C., Lee, B. H. & Park, H. Y. Decoding Arc transcription: a live-cell study of stimulation patterns and transcriptional output. *Learn Mem* **31**, (2024).
83. Suzuki, A., Yanagisawa, M. & Greene, R. W. Loss of *Arc* attenuates the behavioral and molecular responses for sleep homeostasis in mice. *Proceedings of the National Academy of Sciences* **117**, 10547–10553 (2020).
84. Lu, A. T. *et al.* Genetic architecture of epigenetic and neuronal ageing rates in human brain regions. *Nature Communications* **8**, 15353 (2017).
85. Gu, J. *et al.* TC2N maintains stem cell-like characteristics to accelerate lung carcinogenesis by blockade of dual specificity protein phosphatase 3. *Cell Biosci* **15**, 8 (2025).
86. Alvarez-Baron, E. *et al.* RIM3γ and RIM4γ are key regulators of neuronal arborization. *J Neurosci* **33**, 824–839 (2013).
87. Uriu, Y. *et al.* Rab3-interacting molecule gamma isoforms lacking the Rab3-binding domain induce long lasting currents but block neurotransmitter vesicle anchoring in voltage-dependent P/Q-type Ca2+ channels. *J Biol Chem* **285**, 21750–21767 (2010).
88. Tononi, G. & Cirelli, C. Sleep and synaptic down-selection. *Eur J Neurosci* **51**, 413–421 (2020).
89. Mackiewicz, M., Paigen, B., Naidoo, N. & Pack, A. I. Analysis of the QTL for sleep homeostasis in mice: Homer1a is a likely candidate. *Physiol Genomics* **33**, 91–99 (2008).
90. Gould, R. W. *et al.* State-dependent alterations in sleep/wake architecture elicited by the M4 PAM VU0467154 - Relation to antipsychotic-like drug effects. *Neuropharmacology* **102**, 244–253 (2016).
91. Niwa, Y. *et al.* Muscarinic Acetylcholine Receptors Chrm1 and Chrm3 Are Essential for REM Sleep. *Cell Rep* **24**, 2231-2247.e7 (2018).
92. Körber, C., Werner, M., Kott, S., Ma, Z.-L. & Hollmann, M. The transmembrane AMPA receptor regulatory protein gamma 4 is a more effective modulator of AMPA receptor function than stargazin (gamma 2). *J Neurosci* **27**, 8442–8447 (2007).
93. Guo, M.-L. *et al.* CaMKIIalpha interacts with M4 muscarinic receptors to control receptor and psychomotor function. *EMBO J* **29**, 2070–2081 (2010).
94. Wang, Y., Minami, Y., Ode, K. L. & Ueda, H. R. The role of calcium and CaMKII in sleep. *Front Syst Neurosci* **16**, 1059421 (2022).
95. Amrapali Vishwanath, A. *et al.* Mitochondrial Ca2+ efflux controls neuronal metabolism and long-term memory across species. *Nature Metabolism* **8**, 467–488 (2026).

96. Walters, G. C. & Usachev, Y. M. Mitochondrial calcium cycling in neuronal function and neurodegeneration. *Front Cell Dev Biol* **11**, 1094356 (2023).
97. Ren, G. *et al.* CTCF-Mediated Enhancer-Promoter Interaction Is a Critical Regulator of Cell-to-Cell Variation of Gene Expression. *Mol Cell* **67**, 1049-1058.e6 (2017).
98. Davis, L., Onn, I. & Elliott, E. The emerging roles for the chromatin structure regulators CTCF and cohesin in neurodevelopment and behavior. *Cell Mol Life Sci* **75**, 1205–1214 (2018).
99. Klemm, S. L., Shipony, Z. & Greenleaf, W. J. Chromatin accessibility and the regulatory epigenome. *Nature Reviews Genetics* **20**, 207–220 (2019).
100. Mikhail, C., Vaucher, A., Jimenez, S. & Tafti, M. ERK signaling pathway regulates sleep duration through activity-induced gene expression during wakefulness. *Sci Signal* **10**, eaai9219 (2017).
101. Martínez-Zamudio, R. I. *et al.* AP-1 imprints a reversible transcriptional programme of senescent cells. *Nature Cell Biology* **22**, 842–855 (2020).
102. Chen, Y., Chen, L., Lun, A. T. L., Baldoni, P. L. & Smyth, G. K. edgeR v4: powerful differential analysis of sequencing data with expanded functionality and improved support for small counts and larger datasets. *Nucleic Acids Research* **53**, gkaf018 (2025).
103. Kim, S. J. *et al.* Kinase signalling in excitatory neurons regulates sleep quantity and depth. *Nature* **612**, 512–518 (2022).
104. Hyman, S. E., Malenka, R. C. & Nestler, E. J. Neural Mechanisms of Addiction: The Role of Reward-Related Learning and Memory. *Annual Review of Neuroscience* vol. 29 565–598 (2006).
105. Gujar, N., Yoo, S.-S., Hu, P. & Walker, M. P. Sleep Deprivation Amplifies Reactivity of Brain Reward Networks, Biasing the Appraisal of Positive Emotional Experiences. *Journal of Neuroscience* **31**, 4466–4474 (2011).
106. López-Muciño, L. A. *et al.* Sleep loss and addiction. *Neuroscience & Biobehavioral Reviews* **141**, 104832 (2022).
107. Nestler, E. J., Barrot, M. & Self, D. W. DeltaFosB: a sustained molecular switch for addiction. *Proc Natl Acad Sci U S A* **98**, 11042–11046 (2001).
108. McClung, C. A. & Nestler, E. J. Regulation of gene expression and cocaine reward by CREB and ΔFosB. *Nature Neuroscience* **6**, 1208–1215 (2003).
109. ElGrawani, W. *et al.* BDNF-TrkB signaling orchestrates the buildup process of local sleep. *Cell Reports* **43**, (2024).
110. Hammelmann, V. *et al.* Abolishing cAMP sensitivity in HCN2 pacemaker channels induces generalized seizures. *JCI Insight* **4**, 126418 (2019).
111. Rorsman, H. O. *et al.* Sleep pressure accumulates in a voltage-gated lipid peroxidation memory. *Nature* **641**, 232–239 (2025).
112. Gerlai, R. Eph receptors and neural plasticity. *Nature Reviews Neuroscience* **2**, 205–209 (2001).
113. Rasmussen, A. H., Rasmussen, H. B. & Silahtaroglu, A. The DLGAP family: neuronal expression, function and role in brain disorders. *Molecular Brain* **10**, 43 (2017).
114. Mang, G. M. & Franken, P. Sleep and EEG Phenotyping in Mice. *Curr Protoc Mouse Biol* **2**, 55–74 (2012).
115. Buenrostro, J. D., Wu, B., Chang, H. Y. & Greenleaf, W. J. ATAC-seq: A Method for Assaying Chromatin Accessibility Genome-Wide. *Current Protocols in Molecular Biology* **109**, 21.29.1-21.29.9 (2015).

116. Chen, S., Zhou, Y., Chen, Y. & Gu, J. fastp: an ultra-fast all-in-one FASTQ preprocessor. *Bioinformatics* **34**, i884–i890 (2018).
117. Langmead, B. & Salzberg, S. L. Fast gapped-read alignment with Bowtie 2. *Nat Methods* **9**, 357–359 (2012).
118. Dobin, A. *et al.* STAR: ultrafast universal RNA-seq aligner. *Bioinformatics* **29**, 15–21 (2013).
119. Ewels, P., Magnusson, M., Lundin, S. & Käller, M. MultiQC: summarize analysis results for multiple tools and samples in a single report. *Bioinformatics* **32**, 3047–3048 (2016).
120. Gaspar, J. M. Genrich: detecting sites of genomic enrichment. (2018).
121. Broman, K. W. *et al.* R/qtl2: Software for Mapping Quantitative Trait Loci with High-Dimensional Data and Multiparent Populations. *Genetics* **211**, 495–502 (2019).
122. Putri, G. H., Anders, S., Pyl, P. T., Pimanda, J. E. & Zanini, F. Analysing high-throughput sequencing data in Python with HTSeq 2.0. *Bioinformatics* **38**, 2943–2945 (2022).
123. Tyler, A. L. *et al.* Effects of kinship correction on inflation of genetic interaction statistics in commonly used mouse populations. *G3 Genes|Genomes|Genetics* **11**, jkab131 (2021).
124. Rauluseviciute, I. *et al.* JASPAR 2024: 20th anniversary of the open-access database of transcription factor binding profiles. *Nucleic Acids Research* **52**, D174–D182 (2023).
125. Yu, G., Wang, L.-G. & He, Q.-Y. ChIPseeker: an R/Bioconductor package for ChIP peak annotation, comparison and visualization. *Bioinformatics* **31**, 2382–2383 (2015).
126. Cavalcante, R. G. & Sartor, M. A. annotatr: genomic regions in context. *Bioinformatics* **33**, 2381–2383 (2017).
127. Wu, T. *et al.* clusterProfiler 4.0: A universal enrichment tool for interpreting omics data. *The Innovation* **2**, 100141 (2021).
128. Consortium, T. G. O. *et al.* The Gene Ontology knowledgebase in 2023. *Genetics* **224**, iyad031 (2023).
129. Kanehisa, M., Furumichi, M., Sato, Y., Kawashima, M. & Ishiguro-Watanabe, M. KEGG for taxonomy-based analysis of pathways and genomes. *Nucleic Acids Res* **51**, D587–D592 (2023).

Supplementary Files

This is a list of supplementary files associated with this preprint. Click to download.

- FigS3.svg
- TableS5KEAenrichment.xlsx
- FigS4.svg
- FigS9.svg
- TableS8RNAQCsummary.xlsx
- FigS1.svg
- FigS5.svg
- TableS9DifferentialExpression.xlsx
- TableS7GRN.xlsx
- TableS6QTL.xlsx
- FigS8.svg
- FigS7.svg
- FigS6.svg
- FigS2.svg
- TableS3EnrichmentBXD.xlsx
- FigS10.svg
- TableS1ATACQCsummary.xlsx
- TableS2DifferentialCorrelation.xlsx
- TableS4Footprints.xlsx